Electric field in superconductors with rectangular cross section

Ernst Helmut Brandt
Max-Planck-Institut für Metallforschung, Institut für Physik, D-70506 Stuttgart, Germany
(Received 20 April 1995)

The electric field **E** induced in type-II superconductors during the penetration of magnetic flux exhibits a strange profile when the sample has the usual square or rectangular cross section perpendicular to the applied field $B_a(t)$. For example, in the Bean critical state with full penetration of the current density **j**, though $j=j_c$ is constant, **E** is *not* constant but is a linear function of space directed along concentric rectangles (like **j**) with magnitude E exhibiting a zig-zag-folded profile with (a) sharp minima with $E=0$ along the discontinuity lines where the current flow bends, (b) sharp maxima along the median of the short sides, and (c) sharp folds along two lines which are at a distance of half the short side from the short side. This fold defines new discontinuity lines occurring in regions where the current flow is quasihomogeneous. The resulting electric charge density $q=\epsilon_0 \mathrm{div}\mathbf{E}$ is piecewise constant in twelve sections of the rectangle where it is either zero or $q=\pm\epsilon_0 \partial B_a/\partial t$. These exotic features of **E** apply to arbitrary specimen thickness, unlike the current density and the magnetic field, which during flux penetration or exit are qualitatively different in longitudinal and transverse geometries. From a nonlinear diffusion equation, which is local for longitudinal and nonlocal for transverse geometry, the current density, magnetic, and electric fields, vortex velocity, charge density, and local energy dissipation are calculated for penetration and creep of longitudinal or transverse flux in slabs, strips, rectangular bars, and rectangular films or plates of a superconductor which is characterized by a highly nonlinear resistivity.

I. INTRODUCTION

A magnetic field **H** can penetrate into a type-II superconductor in the form of Abrikosov vortices. When the penetrated magnetic field changes with time, an electric field **E** is generated inside the superconductor according to the induction law $\nabla\times\mathbf{E}=-\dot{\mathbf{B}}$ where **B** is the magnetic induction and the dot denotes the time derivative. Inside a type-II superconductor, in general, **B** differs from **H**, while in vacuum or in a nonmagnetic insulator one has $\mathbf{B}=\mu_0\mathbf{H}$. The time variation of **B** may be caused by ramping the applied field $H_a=B_a/\mu_0$ or, when the ramping is stopped and H_a is held constant, by the decay of persistent currents due to the dissipative motion of vortices. The vortices are driven by the Lorentz force density $\mathbf{B}\times\mathbf{j}$ exerted by the circulating persistent currents of density **j**. The resulting vortex motion with velocity **v** induces an electric field $\mathbf{E}=\mathbf{B}\times\mathbf{v}$ which coincides with the electric field obtained from $\nabla\times\mathbf{E}=-\dot{\mathbf{B}}$ if one may disregard the temporal change of the Meissner surface currents flowing within the magnetic penetration depth. The vortex motion is called flux flow or free flux flow when the effects of vortex pinning are negligible[1] (this applies when j or the temperature T are sufficiently large), and it is called flux creep[2] or thermally assisted flux flow[3] (TAFF) when the pins are overcome by thermal activation. By definition, in the TAFF regime (at sufficiently large T) the response E is linear in j, while flux creep leads to a highly nonlinear $E(j)$ curve. For detailed mapping of the E-J-B surface of high-T_c superconductors see Ref. 4.

The electric field inside the superconductor depends on the current density via $\mathbf{E}=\rho\mathbf{j}$. Here ρ is a *scalar* (isotropic) resistivity if one disregards the flux-flow Hall effect, if no current flows along **B**, and if the material is isotropic; else the resistivity is anisotropic and ρ is a tensor. The resistivity in general depends on the induction $B=|\mathbf{B}|$ [e.g., for flux flow $\rho=\rho_{\rm FF}\approx\rho_n B/B_{c2}$ with ρ_n the normal-state resistivity observed above the upper critical field $B_{c2}(T)$], on the temperature T [e.g., for TAFF one has $\rho\approx\rho_{\rm FF}\exp(-U/kT)\ll\rho_{\rm FF}$ where U is an activation energy], and on the current density $j=|\mathbf{j}|$, i.e., $\rho=\rho(j)$ in general is a nonlinear resistivity. The free flux-flow and TAFF regimes are characterized by a linear resistivity $\rho=E/j=$ const, and the flux-creep regime by a highly nonlinear $\rho=E(j)/j=\rho(j)$.[5,6] For example, the Anderson model[7] yields $E(j)=E_c\exp(j/j_c-1)$ and the collective creep[8] and vortex glass[9] or Bose glass[10] models predict $E(j)=E_c\exp[-U(j)/kT]$ with $U(j)=[(j_c/j)^\beta-1]U_0$, where U_0 is a characteristic activation energy, $\beta>0$, j_c is the critical current density, and E_c is defined by $E(j_c)=E_c$. Below the power-law model $E(j)=E_c(j/j_c)^n$ will be used, which describes many experiments and corresponds to an activation energy with logarithmic dependence on j,[11–13] $U=U_0\ln(j_c/j)$, thus $E=E_c\exp[-U(j)/kT]=E_c(j/j_c)^n$ with $n=U_0/kT$.[14] The Bean assumption $j\leqslant j_c$ corresponds to the limit $n\to\infty$ in this power law. The original Bean model[15] makes the three assumptions $n\to\infty$, $j_c(B)=$ const, and longitudinal geometry, i.e., long superconductors in parallel field. Below, all three assumptions shall be relaxed.

In this paper I consider the electric field $\mathbf{E}(\mathbf{r},t)$ induced inside a superconductor by an increasing applied field H_a or by flux creep when no current is applied by contacts. For a superconductor of arbitrary shape, **E** is determined by the induction law $\nabla\times\mathbf{E}=-\dot{\mathbf{B}}$ and by the boundary condition that at the sample surface **E** is along the surface; this follows from $\mathbf{E}=\rho\mathbf{j}$ and from the condition that the current cannot cross the free surface in the absence of contacts. In addition, the electric charge density $q=\epsilon_0\nabla\cdot\mathbf{E}$ should have zero average, i.e., $\langle\mathrm{div}\mathbf{E}\rangle=0$ when the total charge of the sample is

zero. The local charge density, however, in general will not be zero.

The induced electric field determines the local dissipation of energy $p(\mathbf{r})=\mathbf{jE}$. In particular, within the Bean model $j\leqslant j_c$, the local power loss is proportional to $E=|\mathbf{E}|$, namely, $p(r)=j_cE(\mathbf{r})$ since $j=j_c$ in places where $E\neq 0$ and $E=0$ in places where $j<j_c$. Below we will see that within the Bean assumption $j\leqslant j_c$ both in longitudinal and transverse geometry the total dissipation P along the virgin magnetization curve, i.e., for applied field H_a increasing from zero, can be expressed in terms of the total magnetic moment of the sample,

$$\mathbf{m}=\frac{1}{2}\int \mathbf{r}\times\mathbf{j}\, d^3r. \tag{1}$$

Writing $H_a=\hat{\mathbf{z}}H_a(t)$ one has in these geometries for the virgin curve of a superconductor $\mathbf{m}=\hat{\mathbf{z}}m(H_a)$, with $m(0)=0$ and $m(H_a)<0$ for $H_a>0$. The dissipated power $P>0$ may then be written as

$$P=\int \mathbf{jE}\, d^3r=-\dot{B}_a[m(H_a)-H_am'(H_a)]. \tag{2}$$

with $m'=dm/dH_a$. Using $\partial/\partial t=\dot{H}_a\partial/\partial H_a$ and $B_a=\mu_0H_a$ one finds the total dissipated energy $U_{\rm diss}$ along the virgin curve from $P=j_c\int E\, d^3r=\partial U_{\rm diss}/\partial t$,

$$U_{\rm diss}=\mu_0\int_0^{m(H_a)} H\, dm-\mu_0\int_0^{H_a} m\, dH$$

$$=\mu_0H_am(H_a)-2\mu_0\int_0^{H_a} m(H)\, dH. \tag{3}$$

It appears that the expressions (2) and (3) are restricted to the special case $j\leqslant j_c$, $j_c(B)=$ const. In this Bean model the complete magnetization curve in arbitrarily cycled $H_a(t)$ is uniquely determined by the virgin curve $m(H_a)$. In particular, when H_a is cycled between $+H_0$ and $-H_0$ the magnetic moment m_- on the decreasing branch and m_+ on the increasing branch are given by $m_-(H_a)=m(H_0)-2m(H_0/2-H_a/2)$, $m_+(H_a)=-m_-(-H_a)$.[28] The dissipated energy during one cycle of the hysteretic magnetization curve is given by the area of the hysteresis loop, $U_{\rm cycle}=\mu_0\oint m\, dH=\mu_0\oint H\, dm$; this very general thermodynamic result is not restricted to the Bean model.

When the applied field $H_a(t)$ is increased continuously to a sufficiently high value, a superconductor with pinning reaches a critical state in which everywhere in the sample j has reached its maximum value j_c, above which the vortices depin. If the B dependence of j_c is negligible in the range of B values occurring in the sample, then the only contribution to $\dot{\mathbf{B}}$ is from the increasing applied field, $\dot{\mathbf{B}}=\dot{\mathbf{B}}_\mathbf{a}=\mu_0\dot{\mathbf{H}}_\mathbf{a}$.[16] The electric field in the critical state is thus a *universal function* depending only on the sample shape and on the ramp rate $\dot{B}_a$. Moreover, as shown by Gurevich and Küpfer[16] for longitudinal geometry, and by Gurevich and Brandt[17] for transverse geometry, the electric-field profile is universal also during flux creep: When the increase of $H_a(t)$ is stopped at time $t=0$, then $\mathbf{E}(\mathbf{r},t)\approx\mathbf{f}(\mathbf{r})/t$ separates into a universal spatial profile $\mathbf{f}(\mathbf{r})$ and a time dependence $\sim 1/t$. This separation is exact for $E(j)\sim\exp(j/j_1)$ with slabs (strips) or cylinders (disks) in longitudinal (transverse) applied field, but it also is a very good approximation for other specimen shapes and sufficiently nonlinear $E(j)$, e.g., $E\sim j^n$ with $n\geqslant 3$. However, the geometry should be either longitudinal or transverse, i.e., the specimen should have a constant cross section perpendicular to $\mathbf{H_a}\|\hat{\mathbf{z}}$, with parallel extension much larger or much smaller than the perpendicular extension. In these two cases, j, B, and E do not depend on z during the relaxation. This restriction of the universality of flux creep to either long or thin samples, is not required if the quasistatic critical state is considered, i.e., if the ramp rate $\dot{B}_a$ is finite and full penetration was reached.

For homogeneous isotropic slabs, strips, circular cylinders or disks, J, B, and E depend only on one coordinate x or $r=(x^2+y^2)^{1/2}$ and their orientations are obvious from symmetry, $\mathbf{j}\|\hat{\mathbf{y}}$ or $\mathbf{j}\|\hat{\phi}$, $\mathbf{E}\|\mathbf{j}$, and $\mathbf{B}\|\hat{\mathbf{z}}$. The electric field in the critical state is then easily obtained from $\nabla\times\mathbf{E}=-\dot{\mathbf{B}}$, namely,

$$\mathbf{E}(x)=-\dot{B}_a\hat{\mathbf{y}}x \quad \text{(slab, strip)},$$

$$\mathbf{E}(r)=-\dot{B}_a\hat{\phi}r/2 \quad \text{(cylinder, disk)}. \tag{4}$$

For example, $\dot{B}_a=0.002$ T/s and $|x|\leqslant 0.5$ cm yield a maximum $E=10^{-5}$ V/m *inside the superconductor.* The corresponding universal profiles $E(x)$ and $E(r)$ during flux creep are given in Refs. 16 and 17. Remarkably, these creep profiles of E in longitudinal geometry are monotonic, but in transverse geometry they exhibit a maximum at $x/a=1/\sqrt{2}$ and $r/a=0.652$ where a is the strip half-width or disk radius.

In this paper these considerations are extended to superconductors with square or rectangular cross section. We will see that this realistic geometry exhibits some nontrivial features. In particular, discontinuity lines in the current flow will appear which start at the corners of the specimen.[18–21] As an interesting feature I predict discontinuity lines in the electric field E and in its gradient or in the charge density $q=\epsilon_0\mathrm{div}\mathbf{E}$. Some of these lines start on the specimen surface at positions where there is no corner.

The outline of this paper is as follows. The fully penetrated critical state of superconductors with rectangular cross section is described in Sec. II. Partial penetration of flux in the longitudinal and transverse geometries is discussed in Secs. III and IV. For both geometries numerical methods are presented which yield the distribution of J, H, and E by time integration of a nonlinear and local or nonlocal diffusion equation. Some numerical results for square and rectangular cross sections are depicted. The universal profiles of the electric field during flux creep in various geometries are discussed in Sec. V, and a summary is given in Sec. VI.

II. CRITICAL STATE OF SUPERCONDUCTORS WITH RECTANGULAR CROSS SECTION

A. Current density, electric field, drift velocity, local dissipation, and charge density

A superconductor with rectangular cross section $|x|\leqslant a\leqslant b$, $|y|\leqslant b$, and arbitrary extension d along $\hat{\mathbf{z}}\|\mathbf{H_a}$ in the fully penetrated critical state in increasing field has rectangular current stream lines with (Fig. 1)

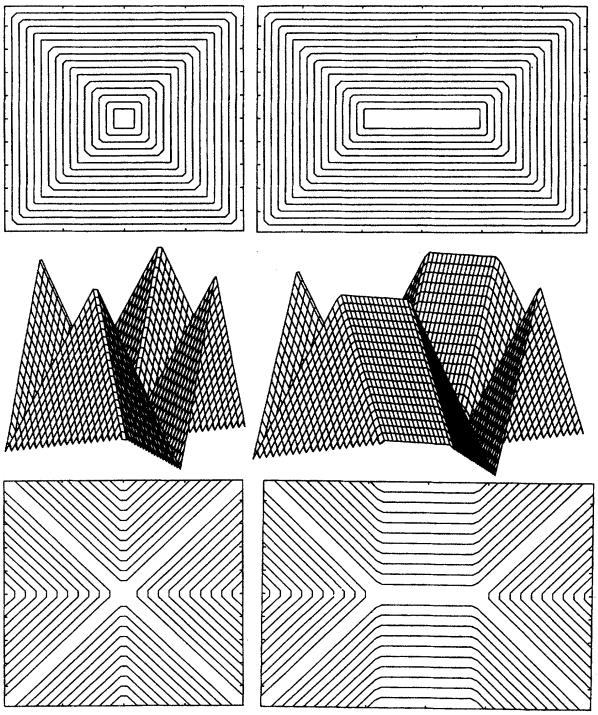

FIG. 1. Current density $\mathbf{j}$ (5) and modulus of the electric field $\mathbf{E}$ (6) inside type-II superconductors with square (*left*) and rectangular (*right*) cross section and arbitrary thickness in the Bean critical state in an increasing magnetic field. Shown are the current stream lines (*top*) and the absolute value E of the electric field as a 3D plot (*middle*) and as contour lines (*bottom*). The local dissipation is $j_c E$ (8) and the vortex velocity is E/B_z (9). The orientation of $\mathbf{E}\|\mathbf{j}$ can be seen from the current stream lines.

$$\mathbf{j}=-j_c\hat{\mathbf{y}}\ \mathrm{sgn}(x) \quad \text{for} \quad |y|<|x|+b-a,$$

$$\mathbf{j}=j_c\hat{\mathbf{x}}\ \mathrm{sgn}(y) \quad \text{for} \quad |y|>|x|+b-a, \tag{5}$$

where $\mathrm{sgn}(x)=x/|x|$. Here and in the following I shall use the abbreviation $s=|y|-|x|+a-b$; the two regions in (5) then correspond to $s<0$ and $s>0$. The electric field satisfying $\mathbf{E}\|\mathbf{j}$ and $(\nabla\times\mathbf{E})\hat{\mathbf{z}}=\partial E_y/\partial x-\partial E_x/\partial y=-\dot{B}_a$ inside the superconductor in this critical state is (Fig. 1)

$$\mathbf{E}=-\dot{B}_a\hat{\mathbf{y}}x \quad \text{for} \quad |y|<b-a,$$

$$\mathbf{E}=\dot{B}_a\hat{\mathbf{y}}s\ \mathrm{sgn}(x) \quad \text{for} \quad |y|>b-a,\ s<0,$$

$$\mathbf{E}=\dot{B}_a\hat{\mathbf{x}}s\ \mathrm{sgn}(y) \quad \text{for} \quad s>0. \tag{6}$$

In particular, for square cross section ($a=b$) one has from (6)

$$\mathbf{E}=\dot{B}_a\hat{\mathbf{y}}\ (|y|-|x|)\ \mathrm{sgn}(x) \quad \text{for} \quad |y|<|x|,$$

$$\mathbf{E}=\dot{B}_a\hat{\mathbf{x}}\ (|y|-|x|)\ \mathrm{sgn}(y) \quad \text{for} \quad |y|>|x|. \tag{7}$$

Note that for the electric field one has 12 qualitatively different regions in the rectangle and eight differing regions in the square, whereas the current flow divides both rectangle and square into only four differing sections. As a new result

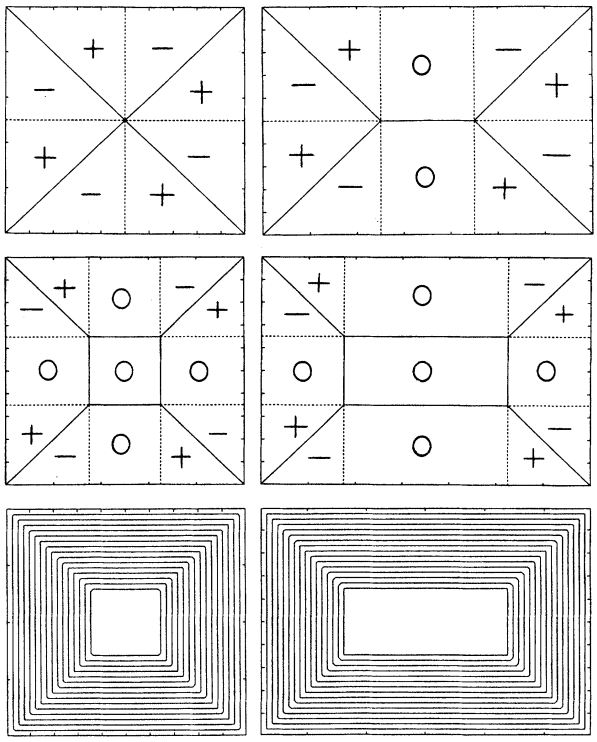

FIG. 2. The electric charge density q (10) inside a square (*right*) and rectangular (*left*) superconductor in increasing magnetic field is piecewise constant. The zeros denote areas with $q=0$, and $\pm$ areas with $q=\pm\epsilon_0\dot{B}_a$. *Top:* Fully penetrated critical state for arbitrary specimen thickness. *Middle:* Partly penetrated state in longitudinal geometry. *Bottom:* The current stream lines or contour lines of the magnetic field in the partly penetrated state in longitudinal geometry.

I obtain that the modulus of the electric field has a sharp fold along the lines $y=\pm(b-a)$, which are not symmetry lines and do not pass through corners.

This electric field of the critical state applies to arbitrary specimen thickness. From $j=j_c$ and $\mathbf{j}\|\mathbf{E}$ follows the local dissipation $p=\mathbf{jE}=j_cE$, which with (6) is

$$p=j_c\,\dot{B}_a\,x \quad \text{for} \quad |y|<b-a,$$

$$p=j_c\,\dot{B}_a|s| \quad \text{for} \quad |y|>b-a. \tag{8}$$

The velocity of the vortices is perpendicular to $\mathbf{j}$ and to $\mathbf{E}=\mathbf{v}\times\mathbf{B}$. Explicitly, one has $\mathbf{v}=\mathbf{E}\times\hat{\mathbf{z}}/B_z$, thus

$$\mathbf{v}=-(\dot{B}_a/B_z)\ \hat{\mathbf{x}}\,x \quad \text{for} \quad |y|<b-a,$$

$$\mathbf{v}=(\dot{B}_a/B_z)\ \hat{\mathbf{x}}\,s\ \mathrm{sgn}(x) \quad \text{for} \quad |y|>b-a,\ s<0,$$

$$\mathbf{v}=-(\dot{B}_a/B_z)\ \hat{\mathbf{y}}\,s\ \mathrm{sgn}(y) \quad \text{for} \quad s>0. \tag{9}$$

Finally, the local charge density $q=\epsilon_0\mathrm{div}\mathbf{E}=\epsilon_0(\partial E_x/\partial x+\partial E_y/\partial y)$ (since $E_z=0$) is from (6) (Fig. 2)

$$q=0 \quad \text{for} \quad |y|<b-a,$$

$$q=-\epsilon_0\dot{B}_a\ \mathrm{sgn}(xys) \quad \text{for} \quad |y|>b-a. \tag{10}$$

In particular, for the square one obtains

$$q=\epsilon_0\dot{B}_a \text{ sgn } [\sin(\phi/4)]. \tag{11}$$

with $\phi=\arctan(y/x)$, i.e., q has constant modulus and alternating sign in eight equal sectors of the square.

These results mean that in a superconducting parallelepiped in the critical state, when the applied field H_a is oriented along one of the edges and is increased further, the magnetic flux penetrates fastest along the middle planes $x=0$ and $y=0$ which are parallel to the sides $x=\pm a$ and $y=\pm b$. As opposed to this, the vortex velocity is zero along the bisector planes $s=|y|-|x|+a-b=0$, $|y|\geq b-a$, which pass through the corners and which coincide with the "discontinuity lines" (or planes)[18–21] at which the current stream lines bend sharply. Note that **E** (6) and **v** (9) are linear functions along all straight lines going through one of the two points $x=0$, $y=\pm(b-a)$ and along all lines which do not cross the lines $y=\pm(b-a)$.

Therefore, in the critical state flux *penetrates mainly from the middle of the edges of the rectangle but not from the corners*, in contrast to what might be expected naively. These results apply to arbitrary thickness. However, for thick specimens in the ideal critical state the dominating flux penetration from the middle of the sides is not obvious in the magnetic-field distribution since the lines of constant $H_z(x,y)$ coincide with the straight rectangular current stream lines; for finite exponent n in $E\sim j^n$, these lines are even concave (barrel-like). But for thin specimens the penetration from the middle of the edges is clearly visible in $H_z(x,y)$ since the lines of constant H_z are convex (starlike or cushionlike). This will be shown now.

B. Magnetic field

While the rectangular current pattern (5) and the electric field (6) in the critical state are *independent* of the specimen thickness d, the magnetic field $\mathbf{H}(x,y,z)$ *does* depend on d. A comprehensive calculation of $\mathbf{H}(x,y,z)$ from the Biot-Savart law was performed by Forkl and Kronmüller[22] for superconductors of various thicknesses d and rectangular and polygonal cross sections. Computations for circular disks of finite thickness are presented in Refs. 23–25. In the limits of large and small d analytical solutions are available:

Large d: In longitudinal geometry, i.e., inside a long bar with rectangular cross section in parallel field, at a sufficient distance away from the ends, one has $\mathbf{H}(x,y,z)\approx\hat{\mathbf{z}}H_z(x,y)$ where $H_z(x,y)$ has the sandpile form with constant slope j_c obtained by Bean.[15] In particular, for rectangular cross section one has

$$H_z=H_a-j_c(a-|x|), \quad s<0,$$

$$H_z=H_a-j_c(b-|y|), \quad s>0, \tag{12}$$

or in compact form, with max(···) = maximum value,

$$H_z=H_a-j_c \max(a-|x|,\ b-|y|). \tag{13}$$

The lines $H_z(x,y)=$ const in this longitudinal geometry coincide with the current stream lines of Fig. 1.

Small d: In thin plates or films with $d\ll a\leq b$ the magnetic field in the critical state depends on d in a trivial way and can be calculated analytically for simple specimen shapes from the known sheet current $\mathbf{J}=\mathbf{j}d=\hat{\mathbf{x}}J_x+\hat{\mathbf{y}}J_y$ and the Biot-Savart law. In general, the parallel components of **H** at the upper surface of a film are $H_x=H_a+J_y/2$, $H_y=H_a-J_x/2$ and at the lower surface $H_x=H_a-J_y/2$, $H_y=H_a+J_x/2$. For rectangular films one has to insert here j_x and j_y from (5). The perpendicular component H_z in the specimen plane $z=0$ inside and outside of the rectangle is obtained by a straightforward calculation,

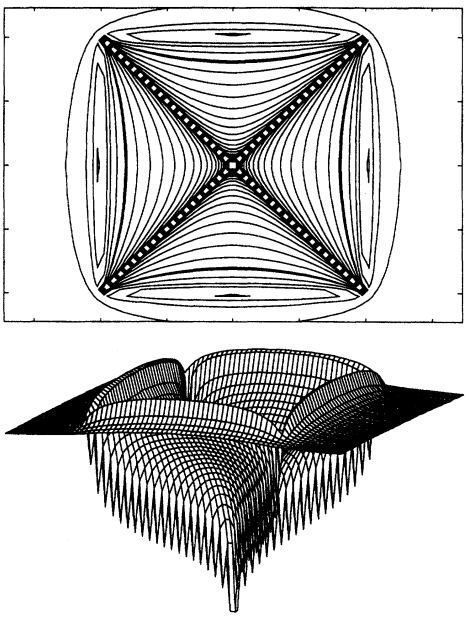

FIG. 3. Contour lines and 3D plot of the magnetic field $H_z(x,y)$ (14) inside and outside a thin square superconductor in the fully penetrated critical state in perpendicular magnetic field. The bold contour line indicates $H_z(x,y)=H_a$.

$$H_z(x,y)=H_a+\frac{J_c}{4\pi}\sum_{p,q=\pm1} f(px,qy),$$

$$f(x,y)=\sqrt{2}\ln\frac{\sqrt{2}P+a+b-x-y}{\sqrt{2}Q-a+b-x-y}+\ln\left|\frac{(P+y-b)(y-b+a)(P+x-a)\,x}{(y-b)(Q+y-b+a)(x-a)(Q+x)}\right| \tag{14}$$

with $P=[(a-x)^2+(b-y)^2]^{1/2}$, $Q=[x^2+(b-a-y)^2]^{1/2}$. This H_z is depicted for $b/a=1$ (square) and $b/a=1.4$ in Figs. 3 and 4. Note the flux concentration in the middle of the edges and the logarithmic infinity of H_z near the discontinuity lines $s=0$ and $x=0$ and near the edges. The "neutral line" $H_z(x,y)=H_a$ is emphasized as a bold line. During flux creep away from the critical state, this neutral line[17,26] separates the inner region where H_z increases, from the outer region where H_z decreases, see Sec. IV.

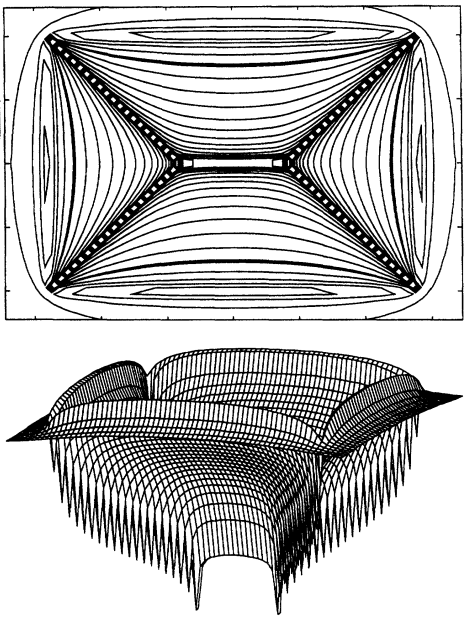

FIG. 4. As Fig. 3 but for a rectangular superconductor with side ratio $b/a=1.4$.

III. FLUX PENETRATION IN LONGITUDINAL GEOMETRY

A. Bean model with $j_c=$const

During flux penetration in increasing applied field, before full penetration is reached, the circulating current and the electric and magnetic fields in general cannot be obtained from such simple arguments as apply for the fully penetrated critical state discussed in Sec. II. An explicit solution for the partly penetrated state is known only for longitudinal slab geometry. For an arbitrary specimen cross section the additional assumption $\mathbf{B}=\mu_0\mathbf{H}$ is required, which is equivalent to zero lower critical field $H_{c1}=0$. For a bar with rectangular cross section $|x|\leq a$, $|y|\leq b$, in the penetrated outer region $|x|\geq x_p$ or $|y|\geq y_p$ the stream lines of the current density $\mathbf{j}(x,y)$ (5) are concentric rectangles and $\mathbf{H}=\hat{\mathbf{z}}H_z(x,y)$ has the shape of the sand pile (13). In the nonpenetrated inner region $|x|<x_p$ and $|y|<y_p$ one has $\mathbf{j}=0$ and $\mathbf{H}=0$. Here $x_p=a-H_a/j_c$ and $y_p=b-H_a/j_c$ denote the distances of the flux fronts from the specimen center.

The electric field which satisfies $\mathbf{E}\|\mathbf{j}$ and $\partial E_y/\partial x-\partial E_x/\partial y=-\dot{B}_a$ in the partly penetrated state is with $s=|y|-|x|+a-b$ from above (Figs. 2, 5–8),

$$\mathbf{E}=0 \quad \text{for} \quad |x|<x_p,\ |y|<y_p,$$

$$\mathbf{E}=\dot{B}_a\hat{\mathbf{y}}[x_p\,\mathrm{sgn}(x)-x] \quad \text{for} \quad |x|>x_p,\ |y|<y_p,$$

$$\mathbf{E}=\dot{B}_a\hat{\mathbf{y}}s\ \mathrm{sgn}(x) \quad \text{for} \quad |y|>y_p,\ s<0,$$

$$\mathbf{E}=\dot{B}_a\hat{\mathbf{x}}s\ \mathrm{sgn}(y) \quad \text{for} \quad |x|<x_p,\ s>0,$$

$$\mathbf{E}=\dot{B}_a\hat{\mathbf{x}}[y-y_p\,\mathrm{sgn}(y)] \quad \text{for} \quad |x|<x_p,\ |y|>y_p. \quad (15)$$

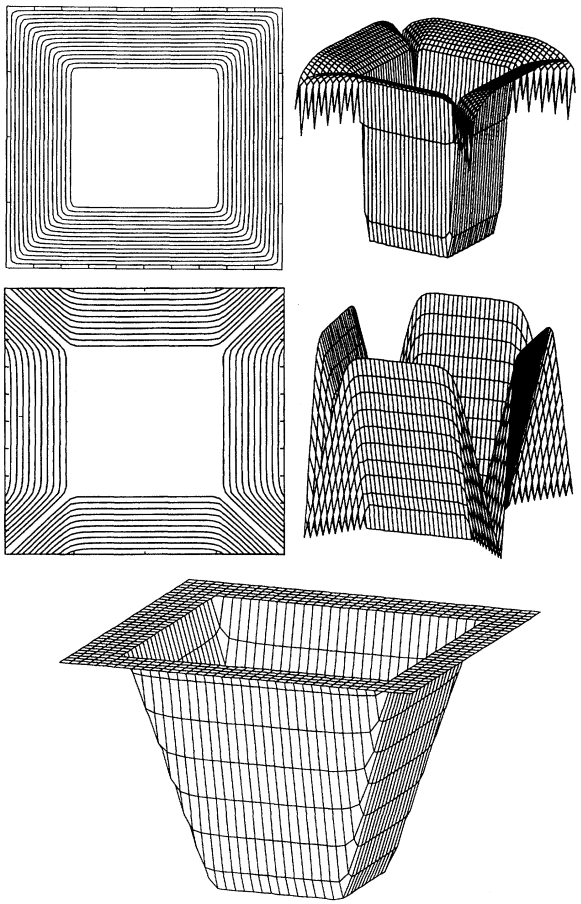

FIG. 5. Partly penetrated state in a square bar in longitudinal field computed from Eq. (23) for the current-voltage law $E=E_c(j/j_c)^n$ with $n=19$ on a grid of $(2\times22)^2$ equidistant points. The depicted state corresponds to $H_a=0.5$ in units j_ca (for the computation one puts $a=E_c=j_c=\dot{H}_a=1$). *Top:* Current stream lines or contour lines of H, and the 3D plot of j. Note the saturation of j to j_c in the penetrated zone and the depression of j to $j_c/\sqrt{2}$ along the diagonals where the current density $\mathbf{j}$ bends by a right angle. *Middle:* Contour lines and 3D plot of the magnitude of the electric field. *Bottom:* The magnetic field $H(x,y)$ inside and outside the bar.

This expression does not simplify much for the square. Note that in the partly penetrated state the electric field divides both the rectangle and the square into 13 different regions, whereas for the current and magnetic field only five different regions may be distinguished. The charge $q=\epsilon_0\mathrm{div}\mathbf{E}$ is zero everywhere except in the squares $|x|>x_p$, $|y|>y_p$ near the corners where one has $p=-\epsilon_0\dot{B}_a\mathrm{sgn}(xys)$ as shown in Fig. 2.

Remarkably, H_z and $\mathbf{E}$ are also known at the two ends of a long bar, namely, they are one half their bulk values (13) and (15), since when two such bars are put together at their ends, the two equal values $H_z(x,y,\pm d/2)$ and $\mathbf{E}(x,y,\pm d/2)$ have to superimpose to give the bulk value. This fact, in principle, allows us to measure the voltage pattern predicted by Eq. (15) by contacts at the ends of a long rectangular specimen.

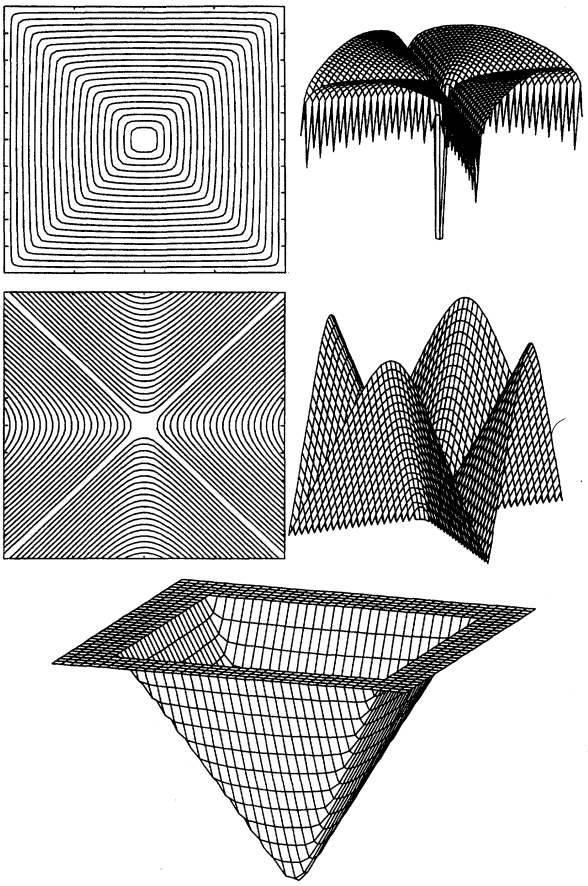

FIG. 6. As Fig. 5 but for the fully penetrated state ($H_a \geq 1$ in units $j_c a$).

The magnetic moment m (1) of the rectangular bar of length d with flux penetrated to a depth $\delta = H_a/j_c$ is

$$m(H_a \leq a j_c) = -2H_a[2ab - (a+b)\delta + \tfrac{2}{3}\delta^2]\, d. \quad (16)$$

($a \leq b$). At full penetration $H_a \geq a j_c$ one has $\delta = a$ and the magnetic moment saturates to the constant value

$$m(H_a \geq a j_c) = m_c = -2 j_c a^2 \left(b - \frac{a}{3}\right) d. \quad (17)$$

The dissipated power P in increasing field is

$$P = 2 j_c \dot{B}_a \delta^2 (b + a - \tfrac{4}{3}\delta)\, d. \quad (18)$$

One easily verifies that the same expression is obtained from the magnetic moment (16) by Eq. (2). The dissipated energy (3) is

$$U_{\text{diss}} = \frac{\mu_0 H_a^2}{j_c}(b + a - \tfrac{8}{9}\delta)\, d. \quad (19)$$

Equations (2) and (3) apply also to a cylindrical bar of radius a. For the cylinder the assumption $j \leq j_c$ yields $j = H = E = 0$ for $r \leq r_p = a - \delta$ with $\delta = H_a/j_c$, and for $r \geq r_p$ one has $j(r) = j_c$, $H(r) = H_a - j_c(r - a)$, and

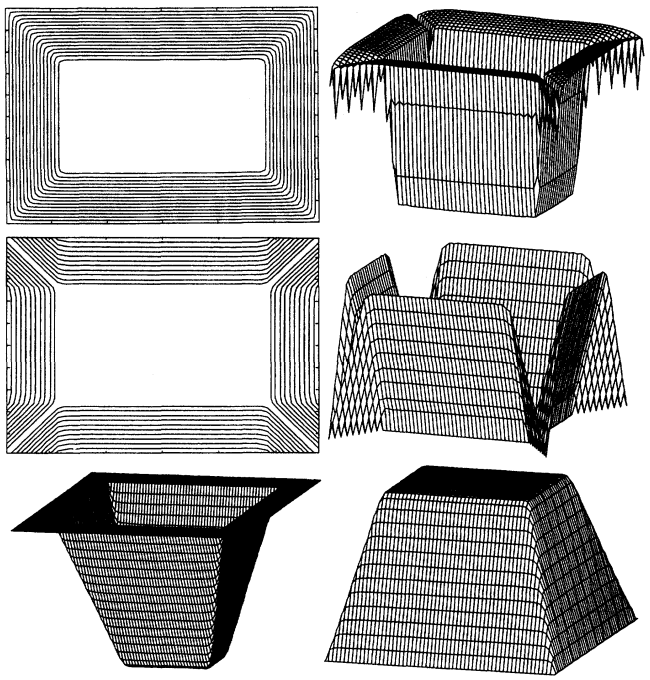

FIG. 7. As Fig. 5 ($H_a = 0.5$) but for a bar with rectangular cross section with $b/a = 1.4$ and for a larger exponent $n = 39$. Also shown is the 3D plot of $-H(x,y)$ inside the superconductor (*bottom, right*).

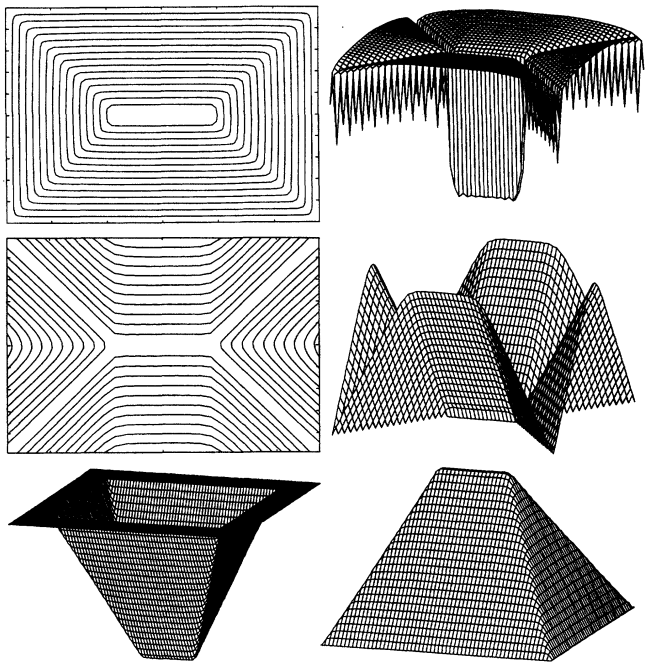

FIG. 8. As Fig. 7 but for full penetration ($H_a \geq 1$).

$$E(r)=\dot{B}_a[r/2-(a-\delta)^2/2r]. \tag{20}$$

The magnetic moment of the cylinder is

$$m(H_a\leqslant aj_c)=-\pi H_a[a^2-a\delta+\delta^2/3]\ d, \tag{21}$$

and the dissipated power and energy are

$$P=\pi j_c\dot{B}_a\delta^2(a-\tfrac{2}{3}\delta),\quad U_{\rm diss}=\frac{\pi\mu_0}{2j_cH_a^2}(a-\tfrac{4}{9}\delta), \tag{22}$$

which again agrees with (2) and (3). Remarkably, the above results for m, P, and $U_{\rm diss}$ coincide for bars with square and circular cross sections if referred to the sample volume.

B. General numerical solution

A useful method to compute the time-dependent penetration, exit, or creep of flux in superconductors with arbitrary cross section in longitudinal geometry goes as follows. Within continuum theory and disregarding the Meissner surface layer and the finite H_{c1} one may write $\mathbf{B}=\mu_0\mathbf{H}=\hat{\mathbf{z}}H_z(x,y,t)$. The electrodynamic behavior of a superconductor in a time-dependent applied field $H_a(t)$ is then completely determined by its nonlinear resistivity $\rho(j,H)$ or, in the TAFF or linear vortex-glass states, by a linear complex resistivity $\rho(\omega)$ which in general depends on the frequency $\omega/2\pi$. From Maxwell's equations one then obtains a very general equation of motion for the current-caused magnetic field $h(x,y,t)=H_z(x,y,t)-H_a(t)$ in longitudinal geometry,

$$\dot{h}(x,y,t)=\nabla\cdot(D\nabla h)-\dot{H}_a(t). \tag{23}$$

In (23) $D=\rho(x,y,t)/\mu_0$ is the flux diffusivity which in general depends on the spatial coordinates x and y and on the time t implicitly via $H(x,y,t)$ and $j(x,y,t)=|\mathbf{j}|=|\nabla h|$, or explicitly when the material is inhomogeneous. For example, one may insert in (23) a nonlinear model resistivity $\rho=\rho_c[j/j_c(x,y)]^{n-1}$ with $n\gg1$ to simulate a superconductor with inhomogeneous pinning. Equation (23) may also be generalized to anisotropic resistivity; for $E_x=\rho_{xx}j_x$ and $E_y=\rho_{yy}j_y$ the gradient term in (23) is replaced by $\nabla_x[\rho_{yy}\nabla_x h]+\nabla_y[\rho_{xx}\nabla_y h]$.

This equation thus, in general, describes the two-dimensional nonlinear diffusion of flux in an inhomogeneous and anisotropic medium, driven by the ramp rate $\dot{H}_a(t)$. In particular, for an ideal conductor with $\rho=0$, Eq. (23) yields $\dot{h}=-\dot{H}_a$, which means that the internal field $H=H_a+h$ stays constant; depending on the initial state, this means frozen-in flux or ideal screening. In the opposite limit of an insulator with $\rho\to\infty$, any finite $h(x,y)$ would diffuse apart rapidly such that $h=0$ results, meaning instantaneous and full penetration of H_a. In the one-dimensional geometries (slab or cylinder) one has $j=|h'|$ (the dash denotes $\partial/\partial x$ or $\partial/\partial r$) and Eq. (23) takes the simple form $\dot{h}=\mu_0^{-1}\nabla\cdot E(|\nabla h|)\nabla h/|\nabla h|-\dot{H}_a$. For a power law $E(j)=E_c(j/j_c)^n$ with odd n one explicitly gets for slabs and cylinders, respectively,

$$\dot{h}(x,t)=c[\ (h')^n\ ]'-\dot{H}_a(t), \tag{23a}$$

$$\dot{h}(r,t)=(c/r)[\ r(h')^n\ ]'-\dot{H}_a(t) \tag{23b}$$

with $c=E_c/j_c^n\mu_0$. For numerical integration of Eq. (23a) and (23b) it is helpful to note that $h(x,t)$ and $h(r,t)$ are *even* functions of x or r which vanish at the surface $|x|=r=a$ and thus may be represented as Fourier series, and that one of the two derivatives acts on an *even* function and one on an *odd* function.

The equation of motion (23) is easily time integrated on a personal computer starting with $h(x,y,0)=0$ and $H_a=0$ and then increasing the applied field $H_a(t)$. Note that only the time derivative $\dot{H}_a$ enters (23) but not the absolute value H_a. For rectangular cross section it is convenient to express $h(x,y)$ in terms of a finite Fourier series which ensures that $h(x,y,t)=0$ at the specimen boundaries and which facilitates the computation of the required spatial derivatives. The accuracy of this numerical method is easily checked by looking at the nonpenetrated region where $h(x,y,t)+H_a(t)=0$ should apply. This is indeed satisfied with high precision even when only few grid points $(x_i,\ y_i)$ or few Fourier coefficients are used. Figures 5 to 8 show some of these numerical results for half and full penetration of longitudinal flux into rectangular bars with side ratios $b/a=1$ and $b/a=2$, using $E=E_c(j/j_c)^n$ with $n=19$ or $n=39$. For such large n the time integration of (23) virtually reproduces the Bean critical state. Note, however, that this computation includes flux-creep effects, which lead to a sweep-rate dependent effective j_c and to magnetic relaxation after the sweep of H_a is stopped, cf. Sec. V.

IV. FLUX PENETRATION IN TRANSVERSE GEOMETRY

A. Long strip with $j_c=$ const

The penetration of perpendicular flux into thin superconductors was recently calculated analytically, within the Bean assumption $j\leqslant j_c$, for thin circular disks[27] and long strips[28] in a transverse field H_a, and for strips carrying a transport current,[29–31] see also the analytical solution for a strip with bulk pinning and edge barrier.[32,33] These theories yield explicit expressions for the sheet current $\mathbf{J}=\mathbf{j}d=\hat{\phi}J(r)$ for the disk and $\mathbf{J}=\hat{\mathbf{y}}J(x)$ for the strip, and for the magnetic moment $\mathbf{m}=\hat{\mathbf{z}}m(H_a)$ in increasing H_a. For the strip, but not for the disk, analytical expressions are also available for the perpendicular field H_z in the specimen plane $z=0$. For a strip with width $2a$ ($|x|\leqslant a$) and length $2b\gg2a$, magnetic flux penetrates to the positions $|x|=x_p$ where $x_p=a/\cosh(H_a/H_c)$ with $H_c=J_c/\pi$, $J_c=j_cd$. One thus has $H_z(x)=0$ for $|x|\leqslant x_p$ and $J_y(x)=-J_c\mathrm{sgn}(x)$ for $x_p\leqslant|x|\leqslant a$. The nontrivial part of the solution[28] may be written in the compact form

$$J_y(x)=-2H_c\ \mathrm{arctan}u,\quad |x|\leqslant x_p, \tag{24}$$

$$H_z(x)=(H_c/2)\ln\left|\frac{1-u}{1+u}\right|,\quad x_p\leqslant|x|<\infty, \tag{25}$$

with $u=cx/|x_p^2-x^2|^{1/2}$ and $c=(1-x_p^2/a^2)^{1/2}=\tanh(H_a/H_c)$. From H_z (25) one finds the electric field $\mathbf{E}=\hat{\mathbf{y}}E_y(x)$ with $E_y(x)=0$ for $|x|\leqslant x_p$ by using the induction law $\partial E_y/\partial x=-\mu_0\partial H_z/\partial t=-\dot{B}_a\partial H_z/\partial H_a$, thus $E_y(x)=-\dot{B}_a\int_{x_p}^{x}[\partial H_z/\partial H_a]\,dx$, yielding (Fig. 9)

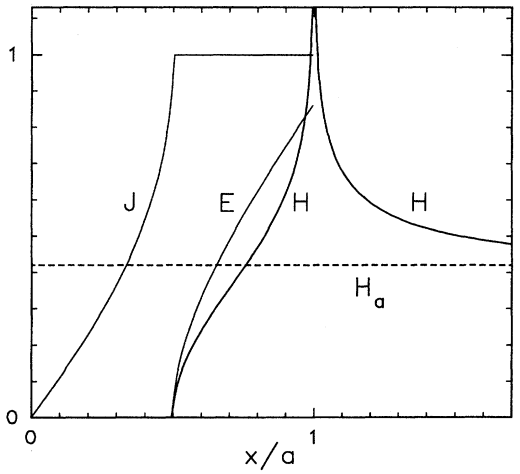

FIG. 9. Sheet current J (24), magnetic field H_z (25), and electric field E (26) for a long strip in perpendicular magnetic field. Shown are $-J/J_c$, H_z/J_c, and $-E/a\dot{B}_a$ for half penetration ($x_p/a=0.5$) occurring at $H_a/J_c=\text{arcosh}2/\pi=0.42$.

$$E_y(x)=-\dot{B}_a\,(x^2-x_p^2)^{1/2}\,\text{sgn}(x),\quad x_p\leq|x|\leq a. \tag{26}$$

From the electric field (26) and the constant current density J_c in the penetrated region $b\leq|x|\leq a$ one obtains the total dissipated power per unit length of the strip, $P/2b=2J_c\int_{x_p}^{a}E_y(x)\,dx$. This yields

$$P(H_a)/2b=J_c\dot{B}_a a^2\left[\tanh\frac{H_a}{H_c}-\frac{H_a/H_c}{\cosh^2(H_a/H_c)}\right]. \tag{27}$$

Noting that the magnetic moment per unit length of the strip is[28]

$$m(H_a)/2b=-J_c\,a^2\,\tanh(H_a/H_c), \tag{28}$$

one confirms that the same dissipation (27) is obtained by inserting $m(H_a)$ (28) into Eq. (2). Thus expressions (2) and (3) apply to both longitudinal and transverse geometries.

B. Numerical solution for strips and disks

If the critical current density depends on B, or if one is interested in the detailed dynamics of flux penetration and exit or creep in long strips in perpendicular field $H_a(t)$, then one may use the following numerical method. First one writes down the perpendicular field component $H_z(x)$ generated in the specimen plane $z=0$ by H_a and by the sheet current $J(x)=j(x)d$ flowing along the strip (along $\hat{\mathbf{y}}$). Using the symmetry $J(-x)=-J(x)$ of the induced sheet current one obtains from Ampère's law

$$H_z(x)=H_a-\frac{1}{2\pi}\int_0^a\frac{2u\;J(u)}{x^2-u^2}\,du. \tag{29}$$

The time-dependent induction $B_z=\mu_0 H_z$ induces an electric field along the strip, $E(x,t)=-\mu_0\int_0^x\dot{H}_z(x,t)\,du$, which drives this sheet current according to $E=\rho J/d$. Eliminating E one gets an equation for $J(x,t)$,[34]

$$J(x,t)=\tau\left[2\pi x\dot{H}_a(t)+\int_0^1 K(x,u)\;\dot{J}(u,t)\;du\right], \tag{30}$$

$$\tau=\frac{ad\mu_0}{2\pi\rho},\quad K(x,u)=\ln\left|\frac{x-u}{x+u}\right|. \tag{31}$$

In (30) the half width a of the strip was used as unit length. The relaxation time τ in general depends on x, J, and H_z via the nonlinear resistivity ρ.

In the equation of motion (30) the time derivative is on the "wrong" side. In order to facilitate the integration over time, this equation has to be inverted such that $\dot{J}$ goes out of the integral. By formally introducing the inverted kernel $K^{-1}(x,u)$ one may solve (30) for $\dot{J}$,

$$\dot{J}(x,t)=\int_0^1 K^{-1}(x,u)\;f(u,t)\;du, \tag{32}$$

$$f(x,t)=J(x,t)/\tau-2\pi x\dot{H}_a(t). \tag{33}$$

In practice the inversion of the integral kernel $K(x,u)$ (31) means the inversion of a matrix $K_{ij}=K(x_i,x_j)w_j$ where the x_i are grid points with weights w_i which approximate an integral by a sum, $\int_0^1 f(x)\,dx\approx\Sigma_{i=1}^{N}f(x_i)w_i$, e.g., $x_i=(i-1/2)/N$ and $w_i=1/N$ with $N=10\ldots100$, see Ref. 32 for details.

The equation of motion (32) is easily integrated on a personal computer starting with $H_a(0)=0$, $J(x,0)=0$, and using a model resistivity, e.g., $\rho(J)=\rho_c(J/J_c)^{n-1}$. From the resulting sheet current $J(x,t)$ one obtains $H_z(x,t)$ by Eq. (29) and the electric field by $E=\rho J/d$.

A similar one-dimensional solution method is described in Ref. 35 for thin circular disks in perpendicular field. Examples for field and current distributions in superconducting disks and rings are given in Refs. 36 and 37 and in Fig. 10. General expressions for the complex ac susceptibility of strips and disks are derived in Refs. 38 and 39.

C. Thin plates of arbitrary shape

A general two-dimensional (2D) equation of motion for the sheet current $\mathbf{J}(x,y,t)=\mathbf{j}d$ in a thin planar conductor or superconductor of thickness d and arbitrary shape in a perpendicular field $\hat{\mathbf{z}}\,H_a(t)$ is derived as follows. As in the longitudinal case (Sec. III B) the material will be characterized by $\mathbf{B}=\mu_0\mathbf{H}$ and by a resistivity $\rho=E/j$ or sheet resistivity $\rho_s=E/J=\rho/d$, which may be nonlinear, e.g., $\rho(j)=\rho_c(j/j_c)^{n-1}$, or linear, complex, and frequency dependent, $\rho=\rho_{ac}(\omega)=\rho'+i\rho''$. The sheet resistivity $\rho_s(x,y)$ may depend on the position either directly in a nonuniform specimen, or implicitly via $J(x,y)$ and $B_z(x,y)$. As in the longitudinal case, planar anisotropy of ρ can be easily incorporated.

First, one expresses the sheet current by a scalar function $g(x,y)$ as

$$\mathbf{J}(x,y)=-\hat{\mathbf{z}}\times\nabla g(x,y)=\nabla\times\hat{\mathbf{z}}\;g(x,y). \tag{34}$$

This substitution guarantees that $\text{div}\mathbf{J}=0$ and that the current flows along the specimen boundary if one puts $g(x,y)=\text{const}=0$ there. In general, the lines $g(x,y)=$ const coincide with the current stream lines. The physical meaning of

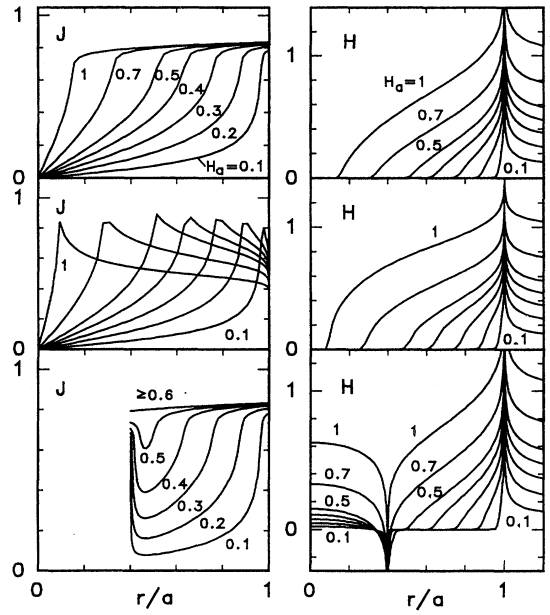

FIG. 10. The penetration of perpendicular flux computed from a 1D integral equation (Ref. 35) similar to Eq. (2), for a circular disk and ring with radius a and thickness $d \ll a$, for $E=E_c[j/j_c(H)]^n$ with $n=19$, and $j_c(H)=j_{c0}=$const or $j_c(H)=j_{c0}/(0.8+|H|)$ (*middle*). Here the perpendicular field $H=H_z$ is in units $j_{c0}d$ ($a=E_c=j_{c0}d=\dot{H}_a=1$). The applied field is increased from zero to $H_a=0.1$, 0.2, 0.3, 0.4, 0.5, 0.7, 1. Shown is the sheet current $J=jd$ (*left*) and the magnetic field H_z for a full disk (*top and middle*) and for a ring with inner radius $0.4a$ (*bottom*).

$g(x,y)$ is the local magnetization or density of tiny current loops. Thus, the integral of $g(x,y)$ over the specimen area yields the magnetic moment (1),

$$\mathbf{m}=\frac{1}{2}\int \mathbf{r}\times\mathbf{J}(\mathbf{r})\, d^2r=\hat{\mathbf{z}}\int g(\mathbf{r})\, d^2r. \tag{35}$$

Next, one determines the integral kernel $Q(\mathbf{r},\mathbf{r}')$ ($\mathbf{r}=x,y$) which relates the perpendicular field $H_z(x,y)$ in the specimen plane $z=0$ to $g(x,y)$ by

$$H_z(\mathbf{r})=H_a+\int_A Q(\mathbf{r},\mathbf{r}')\, g(\mathbf{r}')\, d^2r', \tag{36}$$

$$g(\mathbf{r})=\int_A Q^{-1}(\mathbf{r},\mathbf{r}')\, [H_z(\mathbf{r}')-H_a]\, d^2r'. \tag{37}$$

Here the integrals are over the specimen area A and Q^{-1} is the inverse kernel as discussed below Eq. (32) and (38). Finding the 2D integral kernel Q is not trivial, since when one performs the limit of zero thickness in the Biot-Savart law, the kernel becomes highly singular, $Q=-1/4\pi|\mathbf{r}-\mathbf{r}'|^3$; this form of the kernel thus applies only when $\mathbf{r}$ lies *outside* the specimen, but *inside* the specimen area (where $\mathbf{r}=\mathbf{r}'$ can occur) one should perform part of the integration (36) analytically to obtain a well behaved kernel as described in Ref. 40. Alternatively, one may obtain this kernel numerically for a small but finite height z above the specimen.[41] Knowing that the field of a tiny current loop (or magnetic dipole) of unit strength located at $x=y=z=0$ with axis along z is $H_z(x,y,z)=(1/4\pi)(2z^2-x^2-y^2)/(x^2+y^2+z^2)^{5/2}$, one obtains for the kernel

$$Q(\mathbf{r},\mathbf{r}')=\frac{1}{4\pi}\lim_{z\to 0}\frac{2z^2-\rho^2}{(z^2+\rho^2)^{5/2}} \tag{38}$$

with $\rho^2=(x-x')^2+(y-y')^2$. From Q (38) the inverse kernel Q^{-1} may be obtained by Fourier transform (see below) or by introducing a grid with positions $\mathbf{r}_i=(x_i,y_i)$ and weights w_i, the vectors $H_i=H_z(\mathbf{r}_i)$ and $g_i=g(\mathbf{r}_i)$, and the matrix $Q_{ij}=Q(\mathbf{r}_i,\mathbf{r}_j)w_j$. The integrals (36) and (37) then are approximated by the sums $H_i=\Sigma_j Q_{ij}g_j$ and $g_i=\Sigma_j Q_{ij}^{-1}H_j$ (for $H_a=0$) where Q_{ij}^{-1} is the inverse matrix of Q_{ij}, see also Appendix A.

As the last step, the equation of motion for $g(x,y,t)$ is obtained from the 3D induction law $\nabla\times\mathbf{E}=-\dot{\mathbf{B}}$ and from the material laws $\mathbf{B}=\mu_0\mathbf{H}$ and $\mathbf{E}=\rho\mathbf{j}$, valid inside the sample where $\mathbf{j}=\mathbf{J}/d=-\hat{\mathbf{z}}\times(\nabla g)/d$. Note that the required z component $\dot{B}_z=\hat{\mathbf{z}}\,\dot{\mathbf{B}}=-\hat{\mathbf{z}}(\nabla\times\mathbf{E})=-(\hat{\mathbf{z}}\times\nabla)\,\mathbf{E}=-\hat{\mathbf{x}}\,\partial\mathbf{E}/\partial y+\hat{\mathbf{y}}\,\partial\mathbf{E}/\partial x$ does not depend on the (unknown) derivative $\partial\mathbf{E}/\partial z$. With $\rho_s=\rho/d$ one may write inside the sample $\mathbf{E}=\rho\mathbf{j}=\rho_s\mathbf{J}=-\rho_s\hat{\mathbf{z}}\times\nabla g$ and thus $\dot{B}_z=(\hat{\mathbf{z}}\times\nabla)(\rho_s\hat{\mathbf{z}}\times\nabla g)=\nabla\cdot(\rho_s\,\nabla g)$. Inserting this into Eq. (37) one obtains the equation of motion for $g(x,y,t)$ in the form[42,43]

$$\dot{g}(\mathbf{r},t)=\int Q^{-1}(\mathbf{r},\mathbf{r}')\,[\,f(\mathbf{r}',t)-\dot{H}_a(t)\,]\,d^2r', \tag{39}$$

$$f(\mathbf{r},t)=\nabla\cdot(D_s\,\nabla g), \tag{40}$$

where $D_s=\rho_s/\mu_0=\rho/d\mu_0$ is the sheet diffusivity of flux. Note the similarity of Eqs. (23) and (39), which describe 2D diffusion of magnetic flux in longitudinal and transverse geometry, respectively. In transverse geometry, the diffusion is *nonlocal*, characterized by the integral kernel $Q^{-1}(\mathbf{r},\mathbf{r}')$. In the longitudinal geometry this kernel formally reduces to a delta function $\delta(\mathbf{r}-\mathbf{r}')$ times the specimen thickness d, and $g(\mathbf{r})$ coincides with $H_z(\mathbf{r})-H_a$. In addition, the diffusion in general is *nonlinear* since both Eqs. (23) and (39) apply also when the flux diffusivity ρ/μ_0 depends on $\mathbf{r}$, $\mathbf{J}$, and H_z. When the resistivity is anisotropic ($E_x=\rho_{xx}J_x$, $E_y=\rho_{yy}J_y$) Eq. (39) still applies but with modified

$$f(\mathbf{r},t)=\nabla_x[(\rho_{yy}/d)\nabla_x g]+\nabla_y[(\rho_{xx}/d)\nabla_y g]. \tag{41}$$

In the limit of a long strip or of a rectangle with extreme anisotropy $\rho_{xx}\ll\rho_{yy}$, one can show that Eq. (39) reduces to Eq. (32) for the infinite strip.

D. Rectangular plates

In the particular case of films or plates with rectangular shape, the boundary condition that $\mathbf{J}$ flows along the specimen boundary may be satisfied by writing $g(x,y)$ as a 2D Fourier series in which each term vanishes at the edges. For a rectangle filling the area $0\le x\le 2a$, $0\le y\le 2b$, one writes[42]

$$g(x,y,t)=\sum_{\mathbf{K}} g_{\mathbf{K}}(t)\sin K_x x\sin K_y y, \tag{42}$$

where the $\mathbf{K}$ are reciprocal-lattice vectors with the components $K_x=(2m-1)\pi/2a$ and $K_y=(2n-1)\pi/2b$, $m,n=1,2,3,\ldots$; the sum $\Sigma_{\mathbf{K}}$ is over all $m\geq 1$, $n\geq 1$. A similar Fourier series may be written for the field H_z *inside* the specimen area,

$$H_z(x,y,t)=\sum_{\mathbf{K}} H_{\mathbf{K}}(t)\sin K_x x \sin K_y y. \tag{43}$$

From (36), (42), and (43) one obtains

$$H_{\mathbf{K}}(t)=\sum_{\mathbf{K}'} Q_{\mathbf{K}\mathbf{K}'} g_{\mathbf{K}'}(t), \tag{44}$$

where the $Q_{\mathbf{K}\mathbf{K}'}$ are the 2D Fourier coefficients of the integral kernel Q in Eq. (36),

$$Q(\mathbf{r},\mathbf{r}')=\frac{1}{ab}\sum_{\mathbf{K}\mathbf{K}'} Q_{\mathbf{K}\mathbf{K}'}\sin K_x x \sin K_y y \sin K'_x x' \sin K'_y y' . \tag{45}$$

Explicitly one finds from (38) and (45) (Ref. 42)

$$Q_{\mathbf{K}\mathbf{K}'}=\frac{2}{\pi^2 ab}\int_0^\infty dk_x \frac{K_x K'_x(1+\cos 2ak_x)}{(k_x^2-K_x^2)(k_x^2-K'^2_x)} \times \int_0^\infty dk_y\, k \frac{K_y K'_y(1+\cos 2bk_y)}{(k_y^2-K_y^2)(k_y^2-K'^2_y)} . \tag{46}$$

The integrand in (46) is sharply peaked at $K_x=K'_x$ and $K_y=K'_y$. Without the common factor $k=(k_x^2+k_y^2)^{1/2}$ the double integral (46) would separate and would exactly equal $(1/2)\delta_{\mathbf{K}\mathbf{K}'}$. Therefore, at large K or K' one approximately has $Q_{\mathbf{K}\mathbf{K}'}=\delta_{\mathbf{K}\mathbf{K}'}K/2$. This useful approximation allows to write down the inverse kernel explicitly as $Q^{-1}_{\mathbf{K}\mathbf{K}'}=\delta_{\mathbf{K}\mathbf{K}'}2/K$ and to obtain approximate analytic expressions.

For perpendicular (or normal conducting) rectangular plates or films in increasing, constant, or cycled applied field $H_a(t)$, the magnetization $g(x,y,t)$ may be computed by time integrating the nonlocal diffusion equation (39) with the kernel Q (45, 46) and a material law $E=E(j)$ inserted, see Appendix A for details. From $g(x,y,t)$ the sheet current $\mathbf{J}=\mathbf{j}d=-\hat{\mathbf{z}}\times\nabla g$, magnetic field H (36), and electric field $\mathbf{E}=E(J/d)\hat{\mathbf{J}}$ are obtained. Figures 11–14 show the flux penetration into a square or a rectangle with $b/a=2$ for the model $E=E_c(J/J_c)^n$ ($J_c=j_c d$, $n=19$ or 39) at applied fields $H_a/J_c=0.5$ and $H_a/J_c=1.5$.

V. FLUX CREEP

When the applied field is increased and then held constant at times $t\geq 0$, one has $\dot{H}_a(t)=0$ in Eqs. (23), (33), and (39), which then describe free, nonlinear, and local or nonlocal diffusion of $H(\mathbf{r},t)$ or of $g(\mathbf{r},t)$. As shown by Gurevich,[16,17] in one-dimensional (10) geometries and for sufficiently nonlinear $E(j)$, the electric field $\mathbf{E}(\mathbf{r},t)$ inside the superconductor after some transient time decreases approximately as $1/t$ with a time-independent universal profile from which the current density, magnetic field, and magnetization during flux creep may be obtained by inverting the laws $E=E(j)$ and $\mathbf{j}=\nabla\times\mathbf{H}$.

For *longitudinal geometry* the Maxwell equations

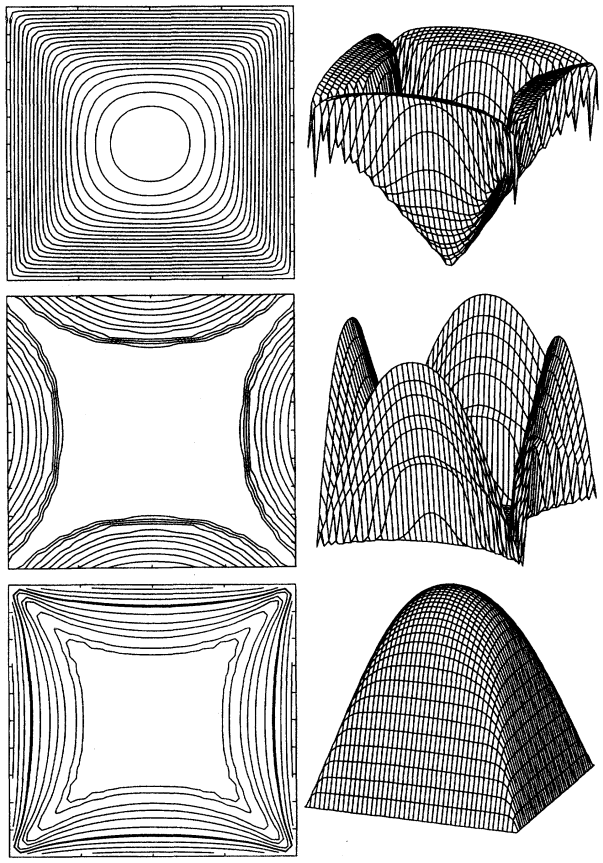

FIG. 11. Penetration of perpendicular magnetic flux into a thin superconducting square with $E=E_c(j/j_c)^n$ for $n=19$ and $H_a=0.5$ in units $j_c d$ ($a=E_c=j_c d=\dot{H}_a=1$) computed from Eq. (39) on a grid with 20×20 basic points. Shown are the current stream lines and a 3D plot of the magnitude of the sheet current (*top*), the contour lines and a 3D plot of the magnitude of the electric field (*middle*), the contour lines of the magnetic field H_z (*bottom, left*) (the bold line indicates $H_z=H_a$), and the local magnetization g (*bottom, right*), whose contour lines coincide with the current stream lines.

$\nabla\times\mathbf{E}=-\dot{\mathbf{B}}$, $\mathbf{B}=\mu_0\mathbf{H}$, $\nabla\times\mathbf{H}=\mathbf{j}=j(E)\hat{\mathbf{E}}$, $\hat{\mathbf{E}}=\mathbf{E}/E$, lead to the equation

$$\nabla\times\nabla\times\mathbf{E}=-\mu_0\,\partial[j(E)\hat{\mathbf{E}}\,]/\partial t. \tag{47}$$

From the boundary condition $B=B_a$ and from $dB_a/dt=0$ follows that at the surface $\nabla\times\mathbf{E}=0$. Neglecting a possible time dependence of the unit vector $\hat{\mathbf{E}}$ and writing $\partial j/\partial t=(\partial E/\partial t)\partial j(E)/\partial E$ one gets for the rather general case where $\partial j(E)/\partial E\approx j_1/E$ [e.g., for $E\sim(j/j_c)^n$ one has $\partial j/\partial E=(j/n)/E\approx j_1/E$ with $j_1=j_c/n$ since for $n\gg 1$ one has $j\approx j_c$ wherever $E\neq 0$]

$$\nabla\times\nabla\times\mathbf{E}=-\mu_0(j_1/E)(\partial E/\partial t)\hat{\mathbf{E}}. \tag{48}$$

This equation is solved by the separation ansatz $\mathbf{E}(\mathbf{r},t)=\mathbf{f}(\mathbf{r})/t$, which is the asymptotic solution for large

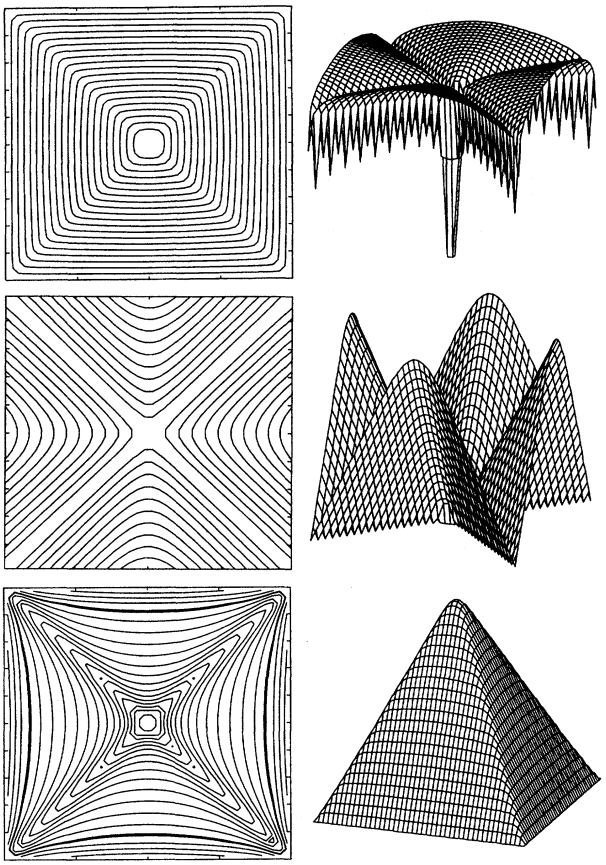

FIG. 12. As Fig. 11 but for almost complete penetration, $H_a = 1.5$.

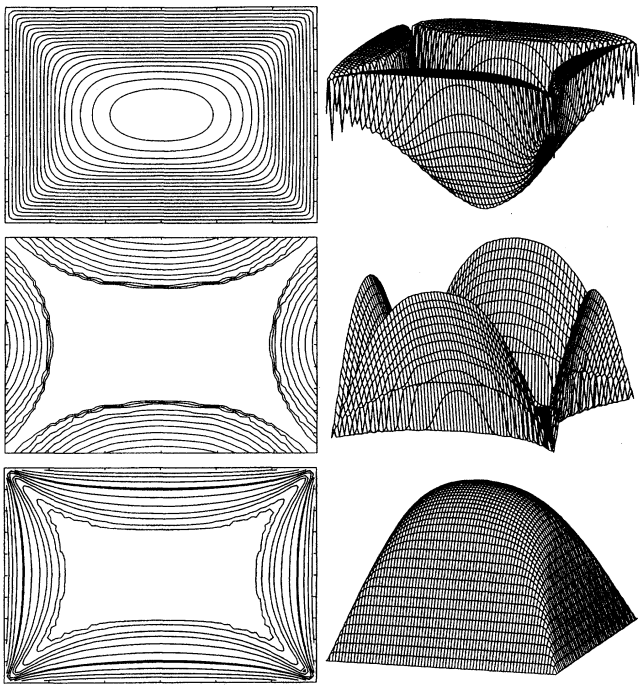

FIG. 13. As Fig. 11 ($H_a = 0.5$) but for a thin rectangular superconductor with $b/a = 1.4$, $n = 39$, and 25×35 basic points.

times since it does not depend on the initial shape $\mathbf{E}(\mathbf{r},0)$. The resulting equations for $\mathbf{f}(\mathbf{r})$ are then

$$\nabla \times \nabla \times \mathbf{f}(\mathbf{r}) = -\mu_0 j_1 \mathbf{f}/f, \quad \nabla \times \mathbf{f}(\mathbf{r})|_{\text{surface}} = 0. \tag{49}$$

This separation of variables is exact for slabs and cylinders in parallel field $H_a \| \hat{\mathbf{z}}$. For slabs with $|x| \leq a$ one has $\mathbf{f}(\mathbf{r}) = \hat{\mathbf{y}} f(x)$, $f''(x) = -\mu_0 j_1 \operatorname{sgn}(x)$, $f'(x = \pm a) = 0$, yielding[16,14]

$$f_{\text{slab}}(x) = \mu_0 j_1 x (a - |x|/2). \tag{50}$$

For circular cylinders with radius a one gets from (49) $\mathbf{f}(\mathbf{r}) = \hat{\phi} f(r)$, $[rf'(r)]' = -\mu_0 j_1 r$, $(rf)'_{r=a} = 0$, yielding

$$f_{\text{cyl}}(r) = \mu_0 j_1 \left[\frac{3a^2 - r_0^2}{4} \frac{\ln(r/r_0)}{\ln(a/r_0) + 1} - \frac{r^2 - r_0^2}{4} \right], \tag{51}$$

where $r_0 \ll a$ is an inner cutoff radius, $f(r_0) = 0$.

For *transverse geometry* the separation of variables is also possible and yields $\mathbf{E}(\mathbf{r},t) = \mathbf{f}(\mathbf{r})/t$. One finds[17] for the strip $\mathbf{f} = \hat{\mathbf{y}} f_{\text{strip}}(x)$ ($|x| \leq a$) and for the disk $\mathbf{f} = \hat{\phi} f_{\text{disk}}(r)$ ($r \leq a$) with

$$f_{\text{strip}}(x) = (\mu_0 j_1 a d/2\pi)[(1+\eta)\ln(1+\eta) - (1-\eta)\ln(1-\eta) - 2\eta \ln \eta], \tag{52}$$

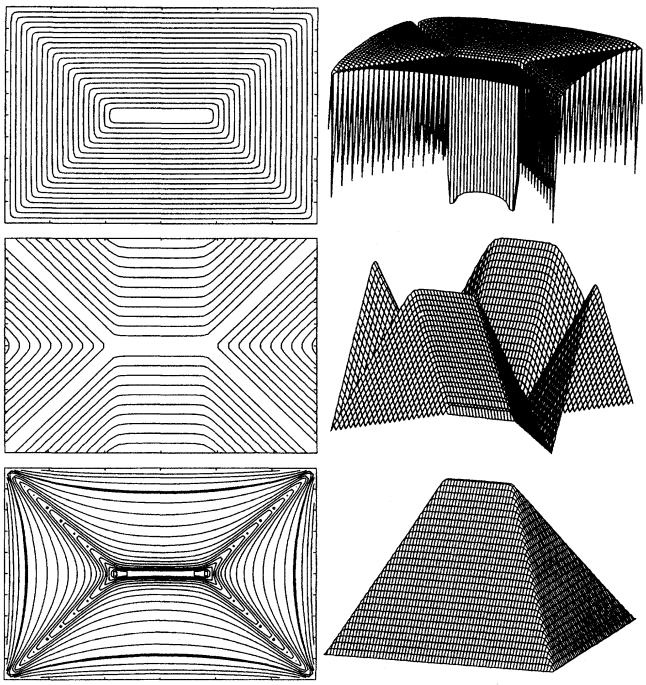

FIG. 14. As Fig. 13 but for almost complete penetration, $H_a = 1.5$.

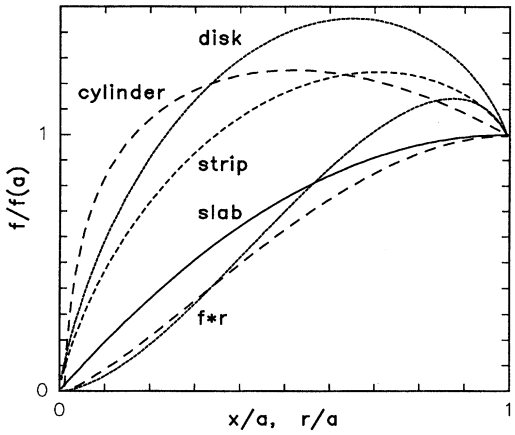

FIG. 15. The universal profiles $f(x)$ and $f(r)$ of the electric field $E=f/t$ induced during flux creep in a slab, cylinder ($r_0=a/100$), strip and circular disk, Eq. (48)–(51), normalized to their values at the specimen edge $x=a$ or $r=a$. Also shown is the product $f(r)r$ for the cylinder and disk.

$$f_{\rm disk}(r)=(\mu_0 j_1 ad/2\pi)[0.4588\eta+0.3731\eta^2-1.5571\eta\ln\eta$$
$$-0.9748(1-\eta)\ln(1-\eta)], \qquad (53)$$

where $\eta=x/a=r/a$. The universal functions $f_{\rm slab}$, $f_{\rm cyl}$, $f_{\rm strip}$, and $f_{\rm disk}$ normalized to their edge value at $x=r=a$ are depicted in Fig. 15. Whereas in longitudinal geometry the flux density during flux creep *increases* uniformly in the entire superconductor, in transverse geometry the perpendicular flux density $B_z=\mu_0 H_z$ increases only in the central part of the superconductor but it *decreases* near the specimen edge since there H_z exceeds H_a due to demagnetization effects. The regions of increasing and decreasing H_z are separated for the strip by a pair of neutral lines at $x=\pm a/\sqrt{2}$ determined by $f'_{\rm strip}(x)=0$, and for the disk by a neutral circle at $r=0.876a$ determined by $[rf_{\rm disk}(r)]'=0$.

The separation of variables, leading to the universality of $\mathbf{E}(\mathbf{r},t)$, is strictly valid only in the four 1D geometries slab, cylinder, strip, and disk as described in Refs. 16 and 17. Remarkably, our computations from Eq. (23) and (39) show that this universal behavior of $\mathbf{E}(\mathbf{r},t)=\mathbf{f}(\mathbf{r})/t$ holds to a very good approximation also for superconductors with rectangular cross section. In all these geometries this universality, in principle, applies to any starting state. However, if the creep does not start from the fully penetrated critical state, then the transient time until the universal shape $\mathbf{E}(\mathbf{r},t)=\mathbf{f}(\mathbf{r})/t$ is reached will be extremely long.

Figures 16 and 17 show the computed electric field induced by the creep of *longitudinal* flux away from the critical state in bars with square and rectangular ($b/a=1.4$) cross section for the model $E(j)\sim j^n$, $n=39$. Note the similarity of these 2D profiles of $E(x,y,t)$ with the 1D parabolic profile (50) in slabs. As a special feature, in square and rectangular superconductors during creep $E(x,y,t)$ stays zero (or extremely small) along the current discontinuity lines discussed in Sec. II. The depicted E profiles do not change over many decades of the creep time t, and their amplitude decreases as $E\sim 1/t$ (more precisely, as $t^{-n/(n-1)}=t^{-39/38}$, see below).

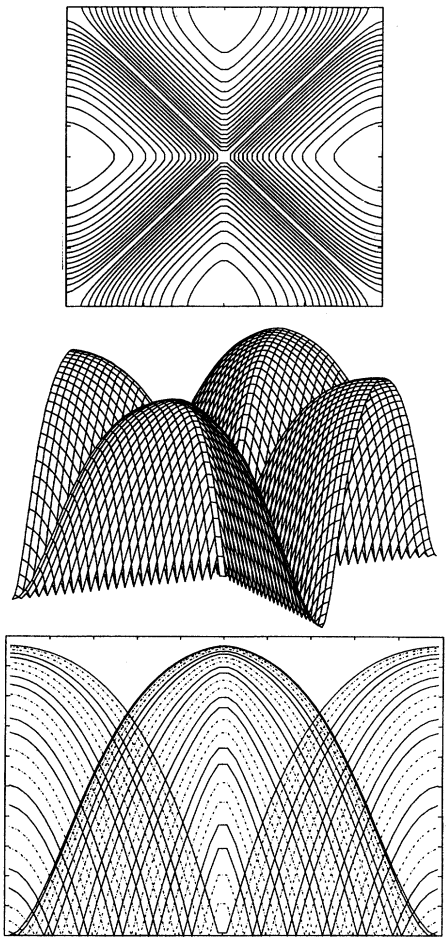

FIG. 16. Universal magnitude of the electric field E during creep of longitudinal flux away from the critical state in a superconducting bar with square cross section and exponent $n=39$, computed from Eq. (23) on a 25×25 grid. *Top:* Contour lines. *Middle:* 3D plot. *Bottom:* Profiles $E(x,y_i)$ cut parallel to the sides of the square.

Note that the time scale of our computation is effectively *logarithmic* since, for numerical stability, the time step was chosen as $\Delta t\sim 1/E_{\rm max}$ where $E_{\rm max}$ is the maximum value of the electric field inside the superconductor; with $E\sim 1/t$ this means $\Delta t\sim t$, yielding a time t which increases exponentially with the number of integration steps.

The creep of *perpendicular* flux away from the critical state in square and rectangular ($b/a=2$) plates or films is depicted in Figs. 18 and 19 for $E(j)\sim j^n$, $n=39$. As in longitudinal geometry, these E profiles stay unchanged over many decades of the creep time. The similarity with the E profiles (52) for the strip is obvious, but on the discontinuity lines of the current one has $E=0$. Note the four or six maxima in E occurring *inside* the square or rectangle, respectively; in *longitudinal* geometry similar maxima occur at the *surface* of the superconductor, cf. Figs. 18 and 19. The neutral lines separating the regions with increasing and decreasing flux density, are now defined by $H_z(x,y)=H_a$;

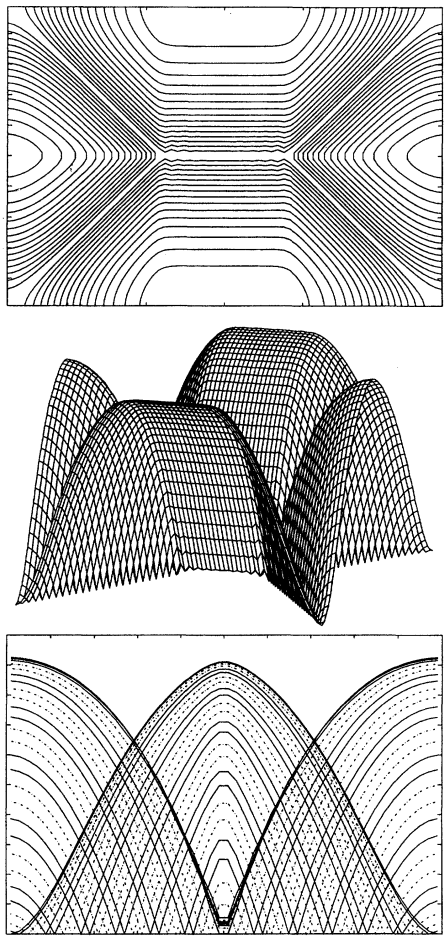

FIG. 17. As Fig. 16 but for a bar with rectangular cross section with $b/a=1.4$ using 25×35 basic points.

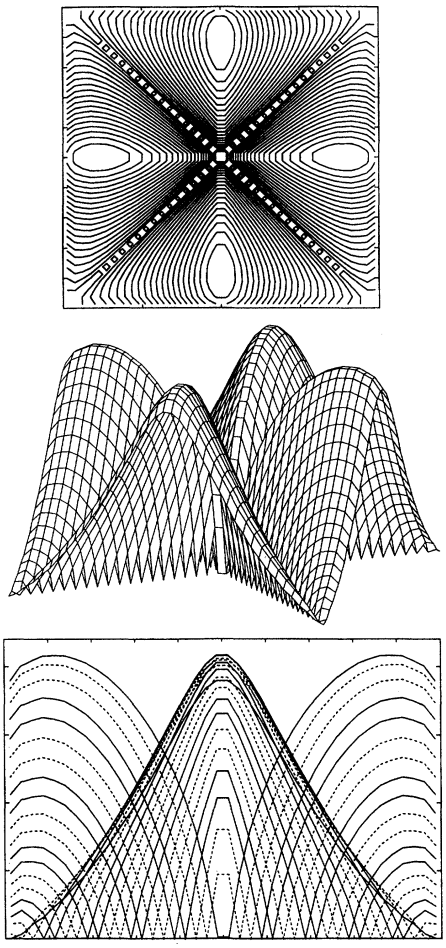

FIG. 18. The magnitude of the electric field during creep of perpendicular flux away from the critical state in a thin superconducting square with exponent $n=39$, computed from Eq. (39) on a 20×20 grid. *Top:* Contour lines. *Middle:* 3D plot. *Bottom:* Profiles $E(x,y_i)$ cut parallel to the sides of the square.

these neutral lines are emphasized as bold lines in the contour plots in Figs. 3, 4, 12, and 14.

During flux creep the current and magnetic-field profiles are close to their profiles in the critical state since the changes of j and H and of the magnetic moment m are approximately logarithmic in time and are thus very slow. More precisely, in our power-law model $E\sim j^n$ with $n=39$ the separation of variables yields $E\sim t^{-n/(n-1)}$ and thus $\Delta H\sim\Delta j\sim\Delta m(t)\sim E^{1/n}\sim t^{-1/(n-1)}=t^{-(1/38)}\approx1-(1/38)\ln t$. These time dependencies are confirmed by our computations over many decades with high precision. Gurevich's universal features of creep[16,17] are thus very general, applying with good accuracy also to geometries and current-voltage laws where the separation of variables in the nonlinear diffusion equation strictly spoken is not valid.

Of course, the nonlinear diffusion equations (23) and (39) allow also the computation of creep away from any partly penetrated state or at any point of the irreversible magnetization curve. Depending on the geometry and magnetic history, such computations yield a plethora of interesting features which cannot be discussed in this paper. The richness of phenomena in perpendicular geometry is increased further when the effects of an edge barrier[32,33,45] or of finite specimen thickness are considered.

VI. SUMMARY AND DISCUSSION

The electric field **E** in type-II superconductors is not zero when the applied field H_a varies with time (even at zero temperature) or when flux creep is considered. Flux creep, observed mainly at high temperatures and when H_a is held constant, is due to a finite and highly nonlinear resistivity of the superconductor. The electric field is induced by moving flux lines and exhibits interesting spatial dependences, which, in principle, may be measured by contacts. The **E** profiles in both longitudinal and transverse geometries are discussed for the fully penetrated critical state, where **E** is a linear function of the spatial coordinate with a strange zigzag profile that is independent of the specimen thickness, and for the more general case of partial penetration of flux. Other cases like a cycled $H_a(t)$ or inhomogeneous or anisotropic superconductors will be discussed elsewhere.

In inhomogeneous superconductors, e.g., with $j_c=j_c(\mathbf{r})$, large peaks of E and of the vortex velocity and local dissipation may occur during flux penetration or exit, which may

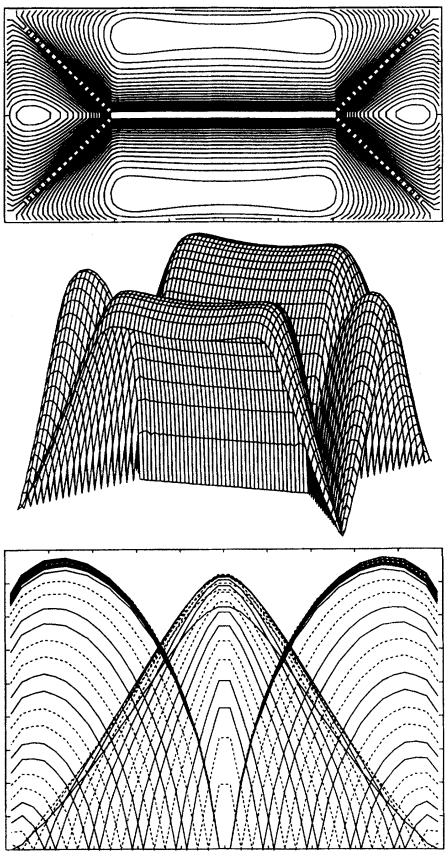

FIG. 19. As Fig. 18 but for a thin rectangular superconductor with side ratio $b/a=2$ on a 20×40 grid.

trigger thermal instabilities.[46] For example, such peaks in E occur along a line leading from the sample edge to an inclusion which destroys the homogeneous current flow, see Fig. 8 of Ref. 21. Sharp peaks and ridges of E occur also when $j_c(\mathbf{r})$ jumps along a straight line such that the critical state exhibits "isolated" triangular regions into which flux lines can enter only through one point on the specimen surface and then move along the jump of j_c, from where they flow at a right angle to the current stream lines into the triangular area; see Ref. 47 for one such example.

The discontinuity lines[18–21] in the current density of rectangular superconductors and the corresponding logarithmic infinities in the flux density in thin films, at finite temperatures have a finite width determined by the curvature of the current-voltage law $E(j)$ near $j=j_c$, e.g., by the exponent n in the model $E=E_c(j/j_c)^n$. The result that E exactly vanishes on the discontinuity lines (even for finite n) means that vortices can never cross these lines since the drift velocity is $v\sim E=0$ on these lines. More precisely, in a rectangle the sheet current on these lines is suppressed from J_c to $J_c/\sqrt{2}$, and thus E is suppressed by a factor of $2^{-n/2}$.

As a result I find discontinuity lines at which the *electric charge density* during flux penetration has a step. A finite charge density $q=\epsilon_0 \mathrm{div}\mathbf{E}$ occurs in regions where the vortex velocity $\mathbf{v}$ has a finite rotation $\nabla\times\mathbf{v}\neq0$. For homogeneous rectangular superconductors q is piecewise constant. This new type of discontinuity lines occurs also in regions where the current flow is quasihomogeneous, e.g., on the two medians of a square-shaped sample. Interestingly, when one takes the nth power of the almost constant current density $j(x,y)$ in the Figs. 5–8 and 11–14, one obtains the zig-zag electric-field profiles shown in the same figures; this should be so since $E\sim j^n$ was assumed in our computations. The nature of these discontinuity lines will be discussed in more detail in a forthcoming paper, where a comparison with the domain structure in soft ferromagnets[48] is given.

General numerical methods are presented which allow the computation of the motion of magnetic flux in square and rectangular (and arbitrarily shaped) superconductors by time integration of a nonlinear diffusion equation. In longitudinal geometry the diffusion (23) of $H(x,y,t)$ is *local*. In transverse geometry the diffusion (39) of the magnetization $g(x,y,t)$ (34) is *nonlocal*, i.e., the time derivative of g depends on the values of ∇g in the entire superconductor.

This numerical method is fast and stable and correctly yields the typical features of thin rectangular superconductors in perpendicular magnetic field,[42] namely, (a) at small H_a the ideal screening state with $1/\sqrt{x}$ singularities of $H(x)$ at the edges of thin plates; (b) at intermediate H_a the cushionlike penetration of flux which was observed magneto-optically;[26,47] and (c) at large H_a the critical state with discontinuity lines at which the current flow performs sharp bends, the flux density exhibits logarithmic infinities, and the electric field goes linearly through zero. The numerical method also allows us to compute the linear and nonlinear response of rectangular superconductors to longitudinal or transverse ac magnetic fields[42] and the exact behavior of a rectangular superconductor performing tilt vibrations.[49–51] In all these cases the superconductor is characterized by a nonlinear resistivity or by a linear, complex, and frequency-dependent resistivity, and the lower critical field H_{c1} is assumed to be zero. Some interesting effects of finite H_{c1} are discussed in Refs. 52 and 53.

The universal behavior of the electric field during flux creep predicted for the 1D geometries in Refs. 16 and 17, is shown to apply to a very good approximation also to superconductors with square and rectangular shape in both longitudinal and transverse geometries. This means that, after some transient time, $\mathbf{E}$ takes the form $\mathbf{E}(\mathbf{r},t)=\mathbf{f}(\mathbf{r})/t$, or more generally, $\mathbf{E}(\mathbf{r},t)=\mathbf{f}(\mathbf{r})/(t+\tau_0)$, where the shape of $\mathbf{f}(\mathbf{r})$ is determined by the geometry. This separation of the variables works whenever the current-voltage law $E(j)$ of the superconductor is sufficiently nonlinear.[16,17] From the universal electric field $\mathbf{E}(\mathbf{r},t)$ one then obtains the creep profiles of the current density $\mathbf{j}$ and the flux density B_z by using the specific law $E(j)$ of the problem.

Magnetization curves $m(H_a)$ of superconductors with rectangular cross section are given for the Bean model in longitudinal geometry by Eq. (16). For transverse geometry $m(H_a)$ has to be computed from Eq. (39). As pointed out by Gilchrist,[54] in the Bean model $j\leqslant j_c=$ const, the magnetization curves for various geometries differ only very little if they are normalized to the same initial slope $m'(0)$ and saturation value $m(\infty)$. In particular, the normalized magnetization curve of the long strip[28] or rectangle[42] exceeds that of the disk[27] by less than $0.011m(\infty)$. I find that the $m(H_a)$ for a thin square differs from that of a circular disk only by

$\pm 0.002m(\infty)$. More details on theoretical magnetization curves and nonlinear susceptibilities of thin rectangles with various current-voltage laws, e.g., $E(j,B)=E_c[\ j/j_c(B)\ ]^n$, will be published elsewhere.

ACKNOWLEDGMENTS

Helpful discussions with Misha Indenbom, John Gilchrist, Aleksander Gurevich, Thomas Schuster, Holger Kuhn, Alexander Forkl, and H. Kronmüller are gratefully acknowledged.

APPENDIX

The computation of current and flux distributions in a rectangular film or plate proceeds as follows. One defines an equidistant grid $x_\mu=(\mu-1/2)a/N_x$ $(\mu=1\ldots N_x)$, $y_\nu=(\nu-1/2)b/N_y$ $(\nu=1\ldots N_y)$. These $N=N_x\times N_y$ points $\mathbf{r_i}=(x_i,y_i)$ $(i=1\ldots N)$ cover one quarter of the rectangle, which suffices because of symmetry. Then one calculates the N^2 Fourier coefficients $Q_{\mathbf{KK'}}$ (46) for N_x values K_x and N_y values K_y, i.e., for $m=1\ldots N_x$, $n=1\ldots N_y$. The N^2 double integrals (46) are computed rapidly by two one-dimensional integrations (or matrix multiplications) if appropriate grids for the k_x and k_y are chosen. Note the symmetry $Q_{\mathbf{KK'}}=Q_{\mathbf{K'K}}$. Next one calculates and tabulates the $N\times N$ symmetric matrix $Q_{ij}=(ab/N)Q(\mathbf{r}_i,\mathbf{r}_j)=Q_{ji}$ from the Fourier series (45). Finally, the inverted matrix Q_{ij}^{-1} is computed and tabulated; this inversion requires $\approx 2\times N^3$ floating point operations and typically takes a few seconds to a few minutes on a personal computer if N_x, $N_y=10$–40 is chosen. For a square specimen the additional symmetry reduces the size of the tabulated matrices by a factor of 4. All these computations have to be performed only once for a given side ratio b/a and grid size $N_x\times N_y$.

Using the tabulated matrices Q_{ij} and Q_{ij}^{-1}, the equation of motion (39) for the vector $g_i(t)=g(x_i,y_i,t)$ is easily integrated over time, starting with $g_i(0)=0$. This was done for various sweep rates $\dot{H}_a(t)$, for cycled $H_a(t)$, and for creep problems ($\dot{H}_a=0$), choosing several current-voltage curves or resistivities $\rho(H,J)$. From the resulting $g(x,y,t)$ one obtains the sheet current $\mathbf{J}(x,y,t)=-\hat{\mathbf{z}}\times\nabla g$ and the magnetic field $H_i(t)=H_z(x_i,y_i,t)=\Sigma_j Q_{ij}g_j$. Both $J=|\nabla g|$ and H are required at each time step since they enter the resistivity, which was chosen in the form $\rho=\rho(x,y,t)=\rho_0[J/J_c(H)]^{n-1}$ where $J=jd$ and $J_c=j_cd$. Even for large exponents $n=99$ the numerical method is quite stable when the spatial derivatives in (40) are calculated from Fourier series of the form (42) using a weak smoothing by multiplication of the Fourier coefficients by a Gaussian. An important trick is that also the spatially constant ramp rate $\dot{H}_a(t)$ is convoluted by a Gaussian to avoid sharp discontinuities at the edges of the rectangle.

A very sensitive check of the accuracy of the numerical method for large exponents $n\gg 1$ is the vanishing of the magnetic field in a wide region inside the rectangle before flux has penetrated: The central field vanishes only when the numerical solution yields a shielding current which exactly compensates the applied field in the field-free region. Any flaw or inaccuracy in the numerics would destroy this compensation. Another test of the accuracy is the constancy of the sheet current in the penetrated region when Bean's assumption $J_c(H)=\text{const}$ is used. In this case a further effective test of the numerical results is the known analytical solution (14) for the fully penetrated critical state which is reached at $H_a\gg J_c$; from the field (29) for the strip, or from the field (14) for the rectangle, one can show that full penetration is reached when $H_a\approx(J_c/\pi)\ln(4a/d)$. In a rectangular superconductor in the critical state the current flows along concentric rectangles since the current cannot cross the surface and must have constant modulus. While our dynamic theory with a smooth current-voltage curve (e.g., $E\sim j^n$ with finite n) yields rounded corners of these rectangular current stream lines, the static Bean model ($j\leqslant j_c$ or $n\to\infty$) gives sharp bends not only near the specimen corners but also inside the specimen.

[1] Y. B. Kim, C. F. Hempstead, and A. R. Strnad, Phys. Rev. **139**, A1163 (1965); M. N. Kunchur, D. K. Christen, and J. M. Phillips, Phys. Rev. Lett. **70**, 998 (1993).

[2] M. R. Beasley, R. Labusch, and W. W. Webb, Phys. Rev. **181**, 682 (1969).

[3] D. Dew-Hughes, Cryogenics **28**, 674 (1988); P. H. Kes, J. Aarts, J. van den Berg, C. J. van der Beek, and J. A. Mydosh, Supercond. Sci. Technol. **1**, 242 (1989).

[4] A. D. Caplin, L. F. Chohen, G. K. Perkins, and A. A. Zhukov, Supercond. Sci. Technol. **7**, 412 (1994); T. K. Worthington, M. P. A. Fisher, D. A. Huse, J. Toner, A. D. Marwick, T. Zabel, C. A. Feild, and F. Holtzberg, Phys. Rev. B **46**, 11 854 (1992).

[5] E. H. Brandt, Z. Phys. B **80**, 167 (1990).

[6] E. H. Brandt, Physica C **195**, 1 (1992).

[7] P. W. Anderson, Phys. Rev. Lett. **9**, 309 (1962); P. W. Anderson and Y. B. Kim, Rev. Mod. Phys. **36**, 39 (1964).

[8] M. V. Feigel'man, V. B. Geshkenbein, A. I. Larkin, and V. M. Vinokur, Phys. Rev. Lett. **63**, 2303 (1989).

[9] M. P. A. Fisher, Phys. Rev. Lett. **62**, 1415 (1989); D. S. Fisher, M. P. A. Fisher, and D. A. Huse, Phys. Rev. B **43**, 130 (1991).

[10] D. R. Nelson and V. M. Vinokur, Phys. Rev. Lett. **68**, 2398 (1992); Phys. Rev. B **48**, 13 060 (1993).

[11] E. Zeldov, N. M. Amer, G. Koren, and A. Gupta, Appl. Phys. Lett. **56**, 1700 (1990).

[12] M. P. Maley and J. O. Willis, Phys. Rev. B **42**, 2639 (1990).

[13] G. Ries, H.-W. Neumüller, R. Busch, P. Kummeth, M. Leghissa, P. Schmitt, and G. Saemann-Ischenko, J. Alloys Compounds **72**, 1268 (1993).

[14] G. Blatter, M. V. Feigel'man, V. B. Geshkenbein, A. I. Larkin, and V. M. Vinokur, Rev. Mod. Phys. **66**, 1125 (1995).

[15] C. P. Bean, Rev. Mod. Phys. **36**, 31 (1964); J. Appl. Phys. **41**, 2482 (1970).

[16] A. Gurevich and H. Küpfer, Phys. Rev. B **48**, 6477 (1993).

[17] A. Gurevich and E. H. Brandt, Phys. Rev. Lett. **73**, 178 (1994).

[18] A. M. Campbell and J. E. Evetts, Adv. Phys. **21**, 199 (1972).

[19] V. K. Vlasko-Vlasov, M. V. Indenbom, V. I. Nikitenko, A. A. Polyanskiĭ, R. L. Prozorov, I. V. Grekhov, L. A. Delimova, I. A. Liniĭchuk, A. V. Antonov, and M. Yu. Gusev, Sverkhprovodi-

most' **5**, 1637 (1992) [Superconductivity **5**, 1582 (1992)].
[20] P. Brüll, D. Kirchgässner, and P. Leiderer, Physica (Amsterdam) **182C**, 339 (1991); Th. Schuster, M. Leghissa, M. R. Koblishka, H. Kuhn, M. Krauss, H. Kronmüller, and G. Saemann-Ischenko, Physica C **203**, 203 (1992).
[21] Th. Schuster, M. V. Indenbom, M. R. Koblishka, H. Kuhn, and H. Kronmüller, Phys. Rev. B **49**, 3443 (1994).
[22] A. Forkl and H. Kronmüller, Physica C **228**, 1 (1994).
[23] M. Daeumling and D. C. Larbalestier, Phys. Rev. B **40**, 9350 (1989).
[24] L. W. Conner and A. P. Malozemoff, Phys. Rev. B **43**, 402 (1991).
[25] H. Theuss, A. Forkl, and H. Kronmüller, Physica C **190**, 345 (1992).
[26] Th. Schuster, H. Kuhn, and E. H. Brandt, Phys. Rev. B **51**, 697 (1995).
[27] P. N. Mikheenko and Yu. E. Kuzovlev, Physica C **204**, 229 (1993); J. Zhu, J. Mester, J. Lockhart, and J. Turneaure, *ibid.* **212**, 216 (1993); J. R. Clem and A. Sanchez, Phys. Rev. B **50**, 9774 (1994).
[28] E. H. Brandt, M. Indenbom, and A. Forkl, Europhys. Lett. **22**, 735 (1993).
[29] W. T. Norris, J. Phys. D **3**, 489 (1970); See, also, G. W. Swan, J. Math. Phys. **9**, 1308 (1968).
[30] E. H. Brandt and M. Indenbom, Phys. Rev. B **48**, 12 893 (1993).
[31] E. Zeldov, J. R. Clem, M. McElfresh, and M. Darwin, Phys. Rev. B **49**, 9802 (1994).
[32] E. Zeldov, A. I. Larkin, V. B. Geshkenbein, M. Konczykowski, D. Majer, B. Khaykovich, V. M. Vinokur, and H. Strikhman, Phys. Rev. Lett. **73**, 1428 (1994); E. Zeldov *et al.*, Physica C **235-240**, 2761 (1994).
[33] I. L. Maksimov and A. A. Elistratov, Pis'ma Zh. Éksp. Teor. Fiz. **61**, 204 (1995) [Sov. Phys. JETP Lett. **61**, 208 (1995)].
[34] E. H. Brandt, Phys. Rev. Lett. **71**, 2821 (1993); Phys. Rev. B **49**, 9024 (1994).
[35] E. H. Brandt, Phys. Rev. B **50**, 4034 (1994).
[36] Th. Schuster, M. V. Indenbom, H. Kuhn, and E. H. Brandt, Phys. Rev. Lett. **73**, 1424 (1994); Th. Schuster, H. Kuhn, E. H. Brandt, M. Indenbom, M. R. Koblischka, and M. Konczykowski, Phys. Rev. B **50**, 16 684 (1994).
[37] E. H. Brandt, Physica C **235-240**, 2939 (1994).
[38] J. Kötzler, G. Nakielski, M. Baumann, R. Behr, F. Goerke, and E. H. Brandt, Phys. Rev. B **50**, 3384 (1994).
[39] E. H. Brandt, Phys. Rev. B **50**, 13 833 (1994).
[40] E. H. Brandt, Phys. Rev. B **46**, 8628 (1992).
[41] P. D. Grant, M. W. Denhoff, W. Xing, P. Brown, S. Govorkov, J. C. Irwin, B. Heinrich, H. Zhou, A. A. Fife, and A. R. Cragg, Physica C **229**, 289 (1994); W. Xing, B. Heinrich, Hu Zhou, A. A. Fife, and A. R. Cragg, J. Appl. Phys. **76**, 4244 (1994).
[42] E. H. Brandt, Phys. Rev. Lett. **74**, 3025 (1995).
[43] E. H. Brandt, Rep. Progr. Phys. (to be published).
[44] V. V. Bryksin and S. N. Dorogovtsev, Physica C **215** 173 (1993).
[45] M. V. Indenbom and E. H. Brandt, Phys. Rev. Lett. **73**, 1731 (1994).
[46] R. G. Mints and A. L. Rakhmanov, Rev. Mod. Phys. **53**, 551 (1981).
[47] Th. Schuster, H. Kuhn, E. H. Brandt, M. V. Indenbom, M. Kläser, G. Müller-Vogt, and H.-U. Habermeier, H. Kronmüller, and A. Forkl, Phys. Rev. B **52**, 10 375 (1995).
[48] H. A. M. van den Berg, J. Appl. Phys. **60**, 1104 (1986).
[49] P. Esquinazi, J. Low Temp. Phys. **85**, 139 (1991).
[50] E. H. Brandt, Phys. Rev. Lett. **68**, 3769 (1992).
[51] M. Ziese, P. Esquinazi, and H. F. Braun, Supercond. Sci. Technol. **7**, 869 (1994).
[52] J. R. Clem and Z. Hao, Phys. Rev. B **48**, 13 774 (1993).
[53] M. V. Indenbom, Th. Schuster, H. Kuhn, H. Kronmüller, T. W. Li, and A. A. Menovsky, Phys. Rev. B **51**, 15 484 (1995).
[54] J. Gilchrist, Physica C **219**, 67 (1994).